High-resolution mantle tomography of China and surrounding regions

Jinli Huang[1,2] and Dapeng Zhao[2]

Received 24 September 2005; revised 13 March 2006; accepted 1 June 2006; published 15 September 2006.

[1] A high-resolution P wave tomographic model of the crust and mantle down to 1100 km depth under China and surrounding regions is determined by using about one million arrival times of P, pP, PP, and PcP waves from 19,361 earthquakes recorded by 1012 seismic stations. The subducting Pacific slab is imaged clearly as a high-velocity zone from the oceanic trenches down to about 600 km depth, and intermediate-depth and deep earthquakes are located within the slab. The Pacific slab becomes stagnant in the mantle transition zone under east China. The western edge of the stagnant slab is roughly coincident with a surface topographic boundary in east China. The active Changbai and Wudalianchi intraplate volcanoes in northeast China are underlain by significant slow anomalies in the upper mantle, above the stagnant Pacific slab. These results suggest that the active intraplate volcanoes in NE China are not hot spots but a kind of back-arc volcano associated with the deep subduction of the Pacific slab and its stagnancy in the transition zone. Under the Mariana arc, however, the Pacific slab penetrates directly down to the lower mantle. The active Tengchong volcano in southwest China is related to the eastward subduction of the Burma microplate. The subducting Indian and Philippine Sea plates are also imaged clearly. The Indian plate has subducted down to 200–300 km depth under the Tibetan Plateau with a horizontal moving distance of about 500 km. High-velocity anomalies are revealed in the upper mantle under the Tarim basin, Ordos, and Sichuan basin, which are three stable blocks in China.

Citation: Huang, J., and D. Zhao (2006), High-resolution mantle tomography of China and surrounding regions, *J. Geophys. Res.*, *111*, B09305, doi:10.1029/2005JB004066.

1. Introduction

[2] China is located in the southeastern portion of the Eurasian continent. Its structure and tectonics are affected by the interaction with three plates: the Pacific, the Philippine Sea and the Indian plates. In the east, the Pacific and the Philippine Sea plates are subducting beneath the Eurasian plate, causing the western Pacific islands arcs, margin seas, and continental rift zones. In the southwest, the India-Asia collision leads to the shortening and elevating of the Tibetan plateau, causing high and great mountain ranges such as the Himalaya, Pamirs, and the Hindu-Kush mountains. The Chinese continent has very complex surface topography, active crustal deformation [*Wang et al.*, 2001], and intensive seismic and volcanic activities. The Earth's highest site (Everest, 8848 m) and the lowest site (Marian trench, −11020 m) are all located in the present study area (Figure 1). This region is surrounded by two strongest seismic belts of the world: the circum-Pacific and the Mediterranean-Himalaya seismic belts. The northern and western parts of China exhibit the strongest intraplate seismic activity in the world. The complex geological structure and tectonics, active crustal deformation and strong seismicity have long attracted attention of geoscientists working in various fields, making it one of the best sites for studying the intraplate tectonics and continental dynamics. Investigation of the three-dimensional (3-D) crust and mantle structure will enable us to better understand the evolution and dynamics of the continent and to clarify the mechanism of intraplate seismicity and volcanism.

[3] Seismic tomography is the most powerful tool to study the heterogeneous structure of the Earth's interior. Since the late 1980s, many researchers have used local earthquake tomography methods to investigate the 3-D crust and upper mantle structure under various regions of China [e.g., *Liu et al.*, 1986, 2000; *Sun and Liu*, 1995; *Huang et al.*, 2002; *Xu et al.*, 2002; *Huang and Zhao*, 2004; *Zhao et al.*, 2004; *Lei and Zhao*, 2005]. *Liu et al.* [1990] and *Liu and Jin* [1993] used regional and distant earthquake data to determine the 3-D P wave velocity structure under China and adjacent regions with a block size of 2–5°. Surface wave data were also used to determine the crust and upper mantle structure under China [e.g., *Zhu et al.*, 2002; *Z. Huang et al.*, 2003]. Pn arrival times were used to investigate the lateral heterogeneity and anisotropy of the uppermost mantle under this region [*Hearn et al.*, 2004; *Liang et al.*, 2004]. Recent global tomographic models provide information on the deep mantle structure under the Chinese

[1]Institute of Earthquake Science, China Earthquake Administration, Beijing, China.
[2]Geodynamics Research Center, Ehime University, Matsuyama, Japan.

0148-0227/06/2005JB004066$09.00

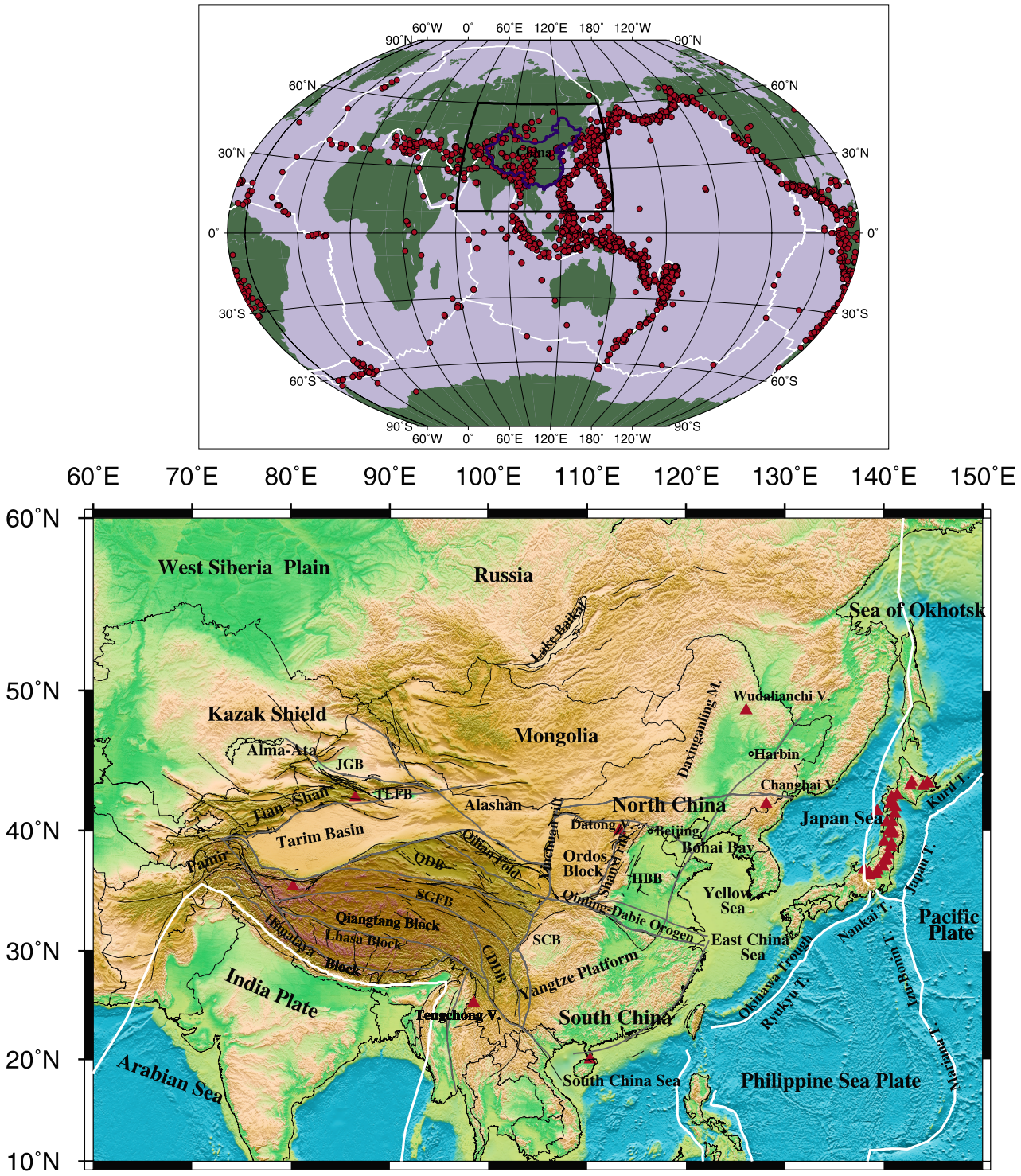

Figure 1. (top) World map showing the location of the present study area. (bottom) Map showing the major geological features of the study area. Color shows the surface topography. White curved lines show the plate boundaries. Grey thin curved lines show the large fault zones and/or tectonic block boundaries in mainland China. Red solid triangles denote volcanoes. Abbreviations are Jungger Basin (JGB), Qaidam Basin (QDB), Sichuan Basin (SCB), Tulufan Basin (TLFB), Songpan Ganzi Fold Belt (SGFB), and Chuandian Diamond Block (CDDB).

region [e.g., *Bijwaard et al.*, 1998; *Zhao*, 2001, 2004]. Although these previous studies have obtained important results on the lateral heterogeneity under China and its surrounding regions, there exist following shortcomings and problems. (1) Because of the limitations in the methodology, data set and computer powers then available, the previous regional tomographic models of China have a lower spatial resolution, which could only reflect the large-scale

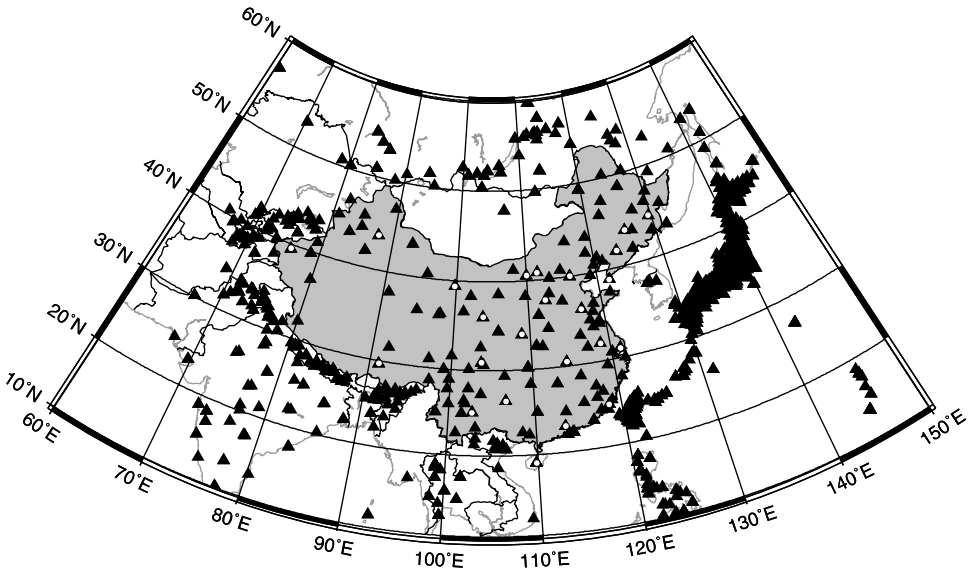

Figure 2. Distribution of seismic stations used in this study. White dots show the ISC stations in China.

structural variations in this region. (2) So far global tomographic studies have mainly used the data set compiled by the International Seismological Center (ISC) which contains only 24 stations in mainland China; hence the spatial resolution of the global tomographic models is very low (4–5° or greater) under China. (3) Because of the long-wavelength nature of the surface wave data, surface wave tomographic models have a lower spatial resolution, which could only reflect the large-scale S wave velocity variations in the study area. (4) Although the local and regional tomographic models for some areas in China have a high spatial resolution, most of them are limited to the shallow upper mantle. Usually, the models for the same area are not consistent with each other due to the differences in the initial model, data set and the method adopted, which have confused the geologists who need the tomographic results for understanding the depth extension of the surface geological features.

[4] In this work we have made great efforts to compile the best Chinese data sets available and used an updated tomographic method to determine a unified, high-resolution, 3-D P wave velocity model down to 1100 km depth under China and its adjacent regions. Compared with the previous studies, our data set contains much more data which were recorded by a large number of seismic stations in mainland China. The tomographic method used [*Zhao*, 2001] enables us to use many later phase data (Pg, Pn, pP, PP, PcP), which greatly improve the ray path coverage in the mantle, leading to a high-resolution tomographic model. Our results shed new light on the deep structure of the different tectonic units in China and their interactions, the fate of the subducting Pacific and Philippine Sea slabs and their effects on the intraplate seismic and volcanic activity and active deformation in east China, as well as the complex structure and tectonics of western China caused by the India-Asia collision.

2. Data and Method

[5] We used four sets of arrival time data extracted from (1) bulletins of the International Seismological Center (ISC) during 1985 to 2000, (2) Annual Bulletin of Chinese Earthquake (ABCE) during 1985 to 2000, (3) reports of the China Digital Seismic Network during 2000 to 2003, and (4) reports of local seismic networks installed in some provinces of China during 1987 to 1997. The ISC data set we used is that reprocessed and released continuously by E. R. Engdahl (the so-called EHB data; see *Engdahl et al.* [1998] for details). For the events reported by both the ISC and other network bulletins, we adopted the hypocentral parameters shown in the EHB data set. There are many events located in mainland China which were recorded by the Chinese seismic networks but not included in the ISC bulletins. For these events, we used the hypocentral parameters accurately relocated by the Chinese seismic networks.

[6] Tremendous efforts were made to process very carefully the huge amount of data sets. The arrival time data for the same events but appeared in the different data sets were merged together, and the repeated and inconsistent data were removed. After this stage of data processing, our data set contains 45,457 events. Then we adopted the following method and criteria to select the final data set for tomographic inversions. The model space is divided into small blocks with a dimension of 0.2° in the latitude and longitude directions and 5 km in depth. Among the events in each block, only one event is selected which has the maximum number of arrival time data (including P, pP, PP and PcP phases) and the most accurate hypocentral location based on the root-mean-square (RMS) traveltime residuals. The selected event was also required to have at least 10 P arrival time pickings. Our final data set thus selected contains 978,769 arrival times from 19,361 events recorded by 1012 seismic stations. The arrival times include 839,629 P, 30,128 PcP, 76,020 pP and 32,992 PP phases. Figures 2 and 3 show the seismic stations and events used in this study, respectively. It is clear that there are many stations and earthquakes in and around the Japan Islands and the Taiwan region. The distribution of events and stations is also good in east China, Tianshan region in western China, and the India-China boundary region. Thus tomographic

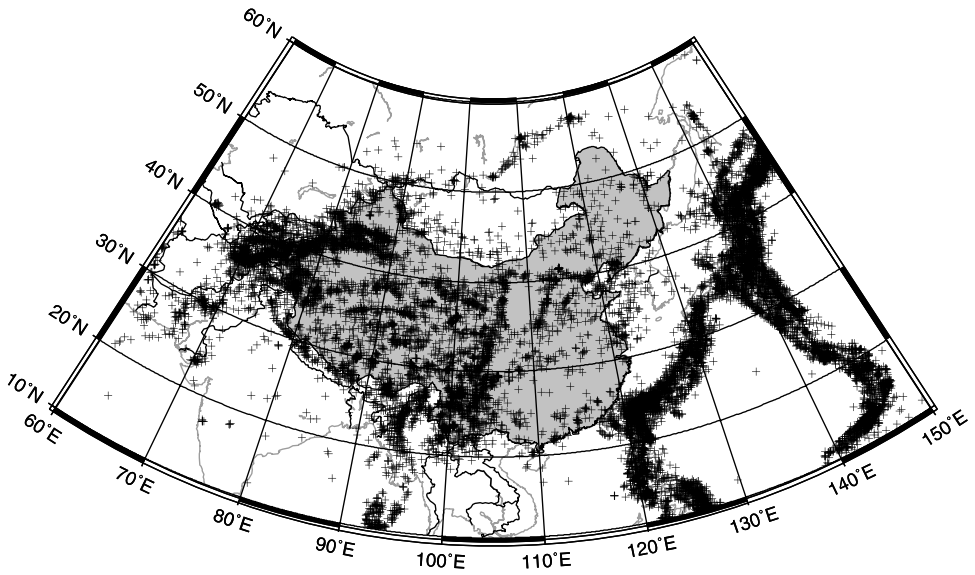

Figure 3. Epicentral distribution of earthquakes used in this study.

images under these well-sampled regions would have a high resolution. Although there are few stations in the Tibetan region, the dense distribution of earthquakes makes the ray path coverage there very good. For some regions such as Mongolia and Philippines where both seismic stations and events are scarce, the use of later phases (e.g., pP, PP) is important to improve the ray coverage there.

[7] To analyze our data set, we used the tomographic inversion method of *Zhao* [2001]. Three-dimensional grid nodes were set up in the modeling space. The grid spacing in the horizontal direction is 1° except for the edge portions of the study region. In the depth direction the grid spacing is 15 to 100 km in the crust and upper mantle, and 200 to 300 km in the lower mantle. Thus the number of grid nodes is 48, 89 and 19 in the latitude, longitude and depth directions, respectively. Velocity perturbations at the grid nodes are taken as unknown parameters. The velocity perturbation at any point in the modeling space is calculated by linearly interpolating the velocity perturbations at the eight grid nodes surrounding that point. Figure 4 shows the one-dimensional (1-D) velocity model we adopted for the 3-D tomographic inversion. The 1-D model is derived from the iasp91 Earth model [*Kennett and Engdahl*, 1991] with an average crustal velocity of 6.3 km/s and a Moho depth of 45 km by referring to the results of many deep seismic sounding studies conducted in the Chinese continent [see *Li and Mooney*, 1998]. Ray paths and traveltimes are computed accurately by using an efficient 3-D ray tracing method [*Zhao et al.*, 1992; *Zhao and Lei*, 2004]. The LSQR algorithm [*Paige and Saunders*, 1982] with damping and smoothing [*Zhao*, 2001] was used to solve the large and sparse observational equations that relate the arrival time data to the unknown velocity parameters. Only the arrival time data with traveltime residuals smaller than 5 s were used in the inversion. Only the grid nodes with hit counts more than 10 were included for inversion, while the actual hit counts are hundreds or greater for most of the grid nodes. The number of traveltimes actually used in the inversion is 930,037, and the number of inverted grid nodes is 53,423.

[8] We conducted many tomographic inversions using different values of damping parameter. Considering the balance between the data variance reduction and the smoothness of the obtained 3-D velocity model, we found the best value of damping parameter is 40.0. The RMS traveltime residual is 2.463 s before the inversion, and it was reduced to 1.523 s after the inversion. The variance reduction is 62%.

3. Checkerboard Resolution Tests

[9] To confirm the main features of the tomographic result, we conducted detailed resolution analyses. A direct

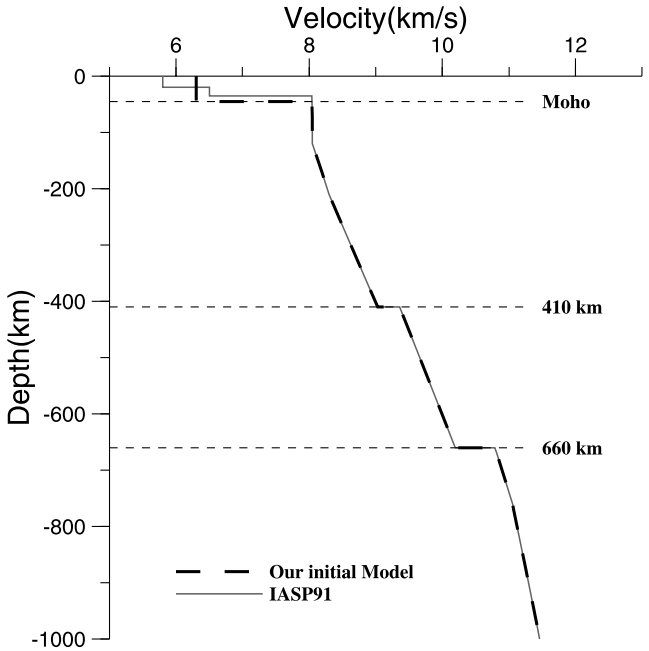

Figure 4. Initial velocity model (dashed lines) modified slightly from the iasp91 Earth model (grey lines).

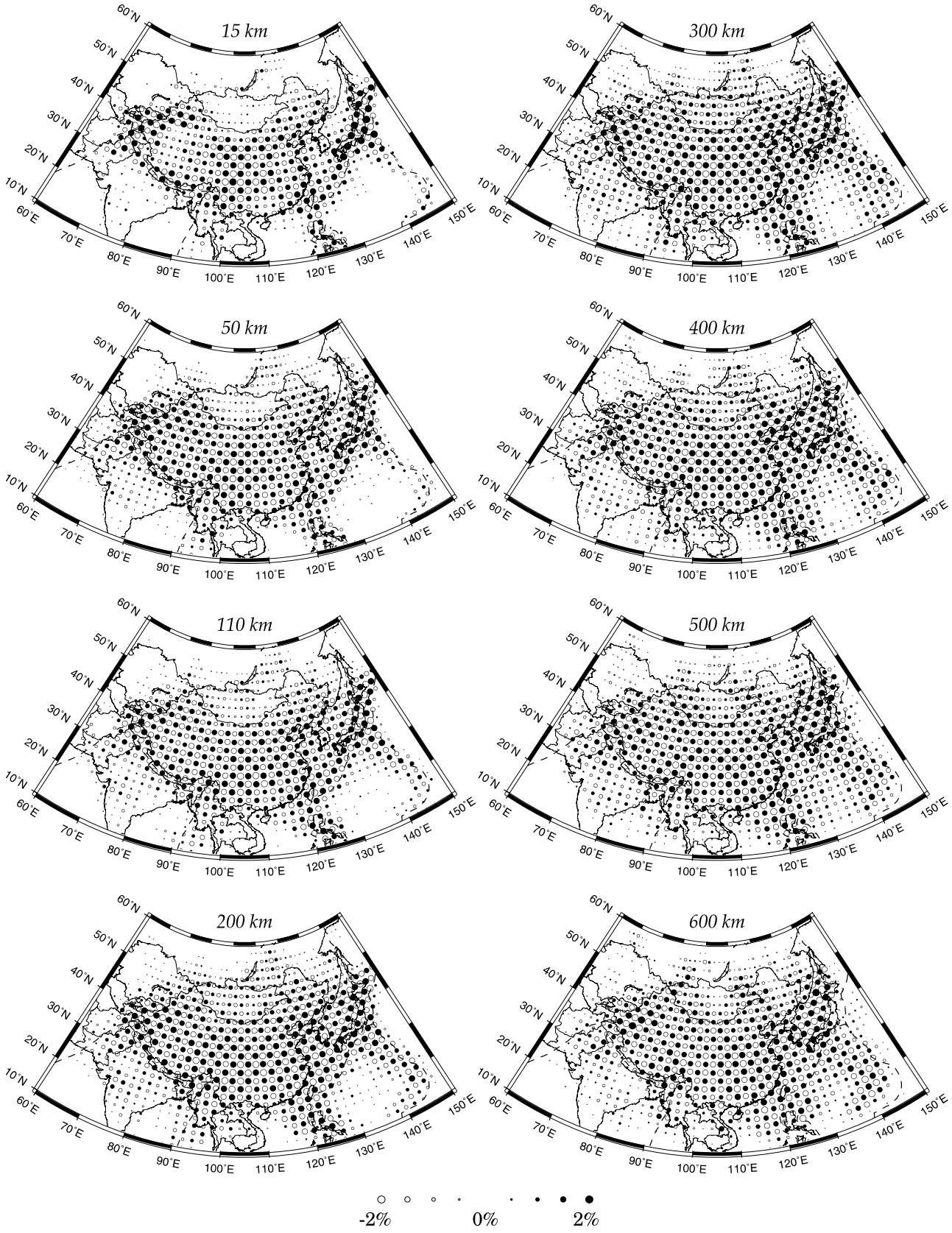

Figure 5. Results of checkerboard resolution test when a 2° × 2° grid was adopted. The depth of the layer is shown on the top of each map. Solid and open circles denote high and low velocities, respectively. The velocity perturbation scale is shown at the bottom.

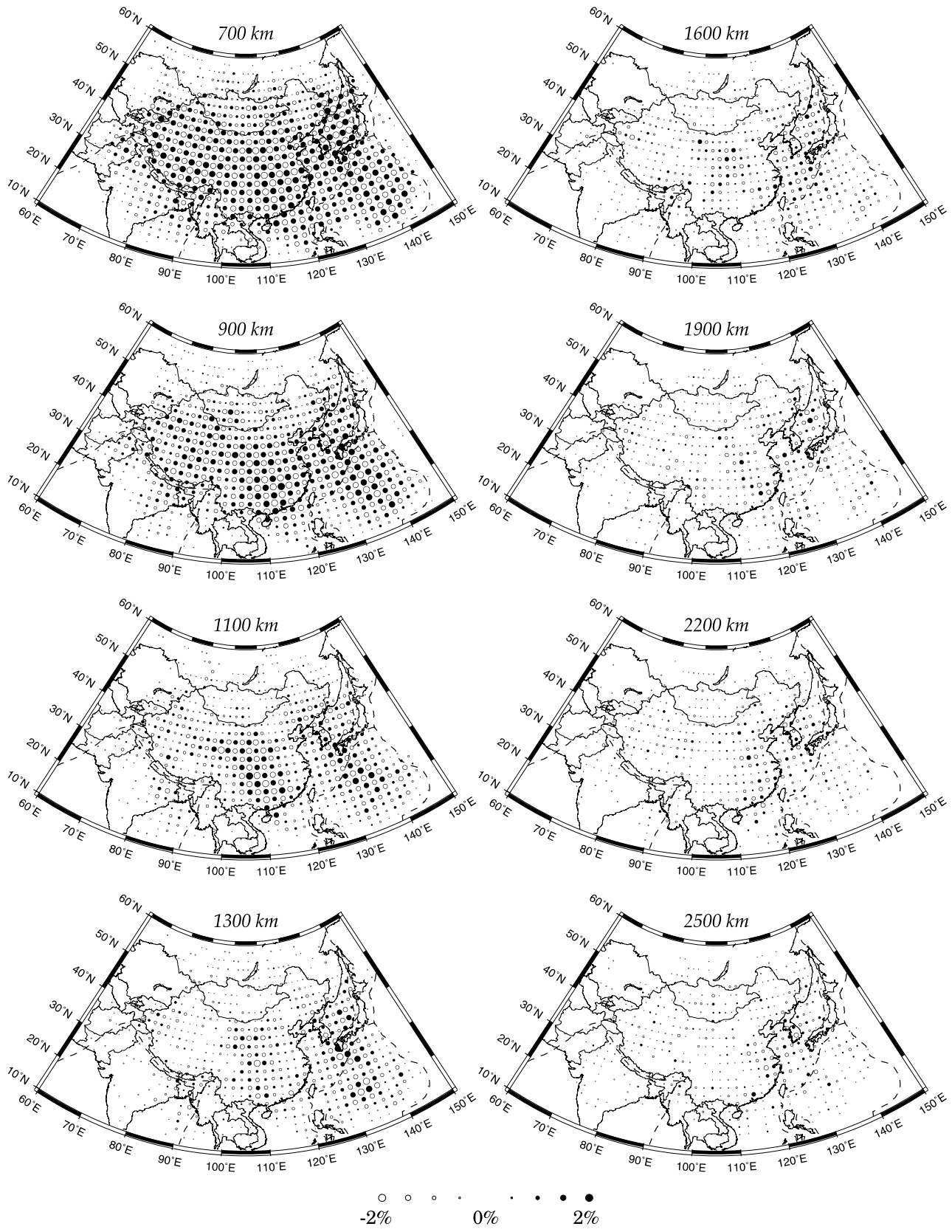

Figure 5. (continued)

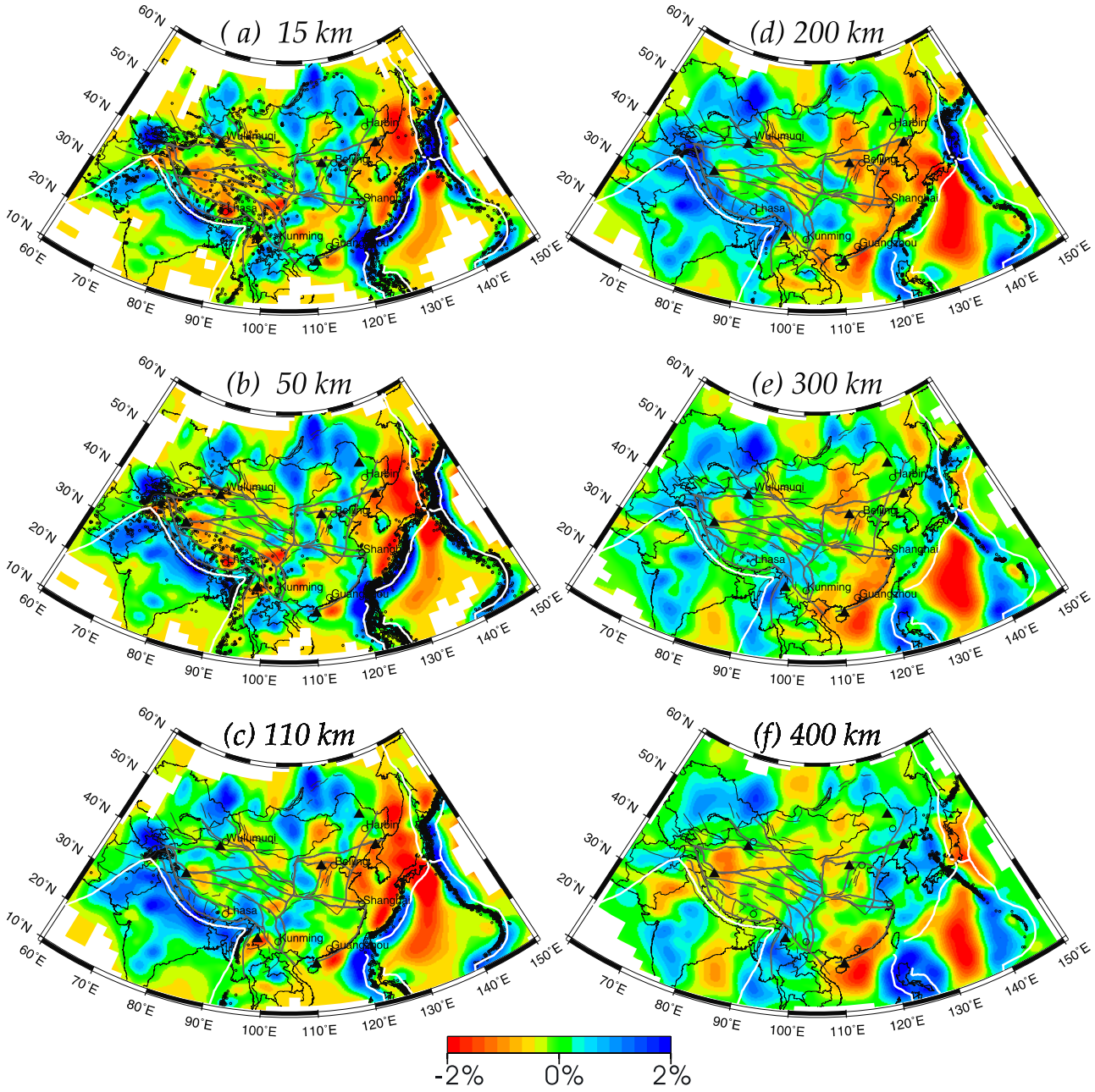

Figure 6. P wave velocity image at each depth slice (in percent from the average velocity). The depth of each layer is shown on the top of each map. Red and blue colors denote low and high velocities, respectively. Black dots show earthquakes occurred from 1964 to 2003 relocated by *Engdahl et al.* [1998]. The velocity perturbation scale is shown at the bottom. Other labels are the same as those in Figure 1.

way to evaluate the resolution of a tomographic result is to conduct synthetic tests. The procedure to conduct a synthetic test is as follows. First a synthetic velocity model was constructed. Then synthetic arrival times were calculated for the synthetic model with the same numbers of earthquakes, stations and ray paths as those used for the inversion of the real data. Finally these synthetic arrival times were inverted by using the same algorithm as that used for the inversion of the real data. Comparing the synthetic model with its reconstructed image, we can judge where the resolution is good and where it is poor. In this study we conducted two kinds of synthetic tests. One is the checkerboard resolution tests, the other is restoring tests for the stagnant slab.

[10] The checkerboard resolution test [*Zhao et al.*, 1992; *Leveque et al.*, 1993] is just a special form of synthetic test. The only difference between them is in the input model. To make a checkerboard, positive and negative velocity perturbations (2%) are assigned to the 3-D grid nodes that are arranged in the modeling space, the image of which is straightforward and easy to remember. From the checkerboard results, one can know the variation of the spatial resolution in the whole study region. In this work, we

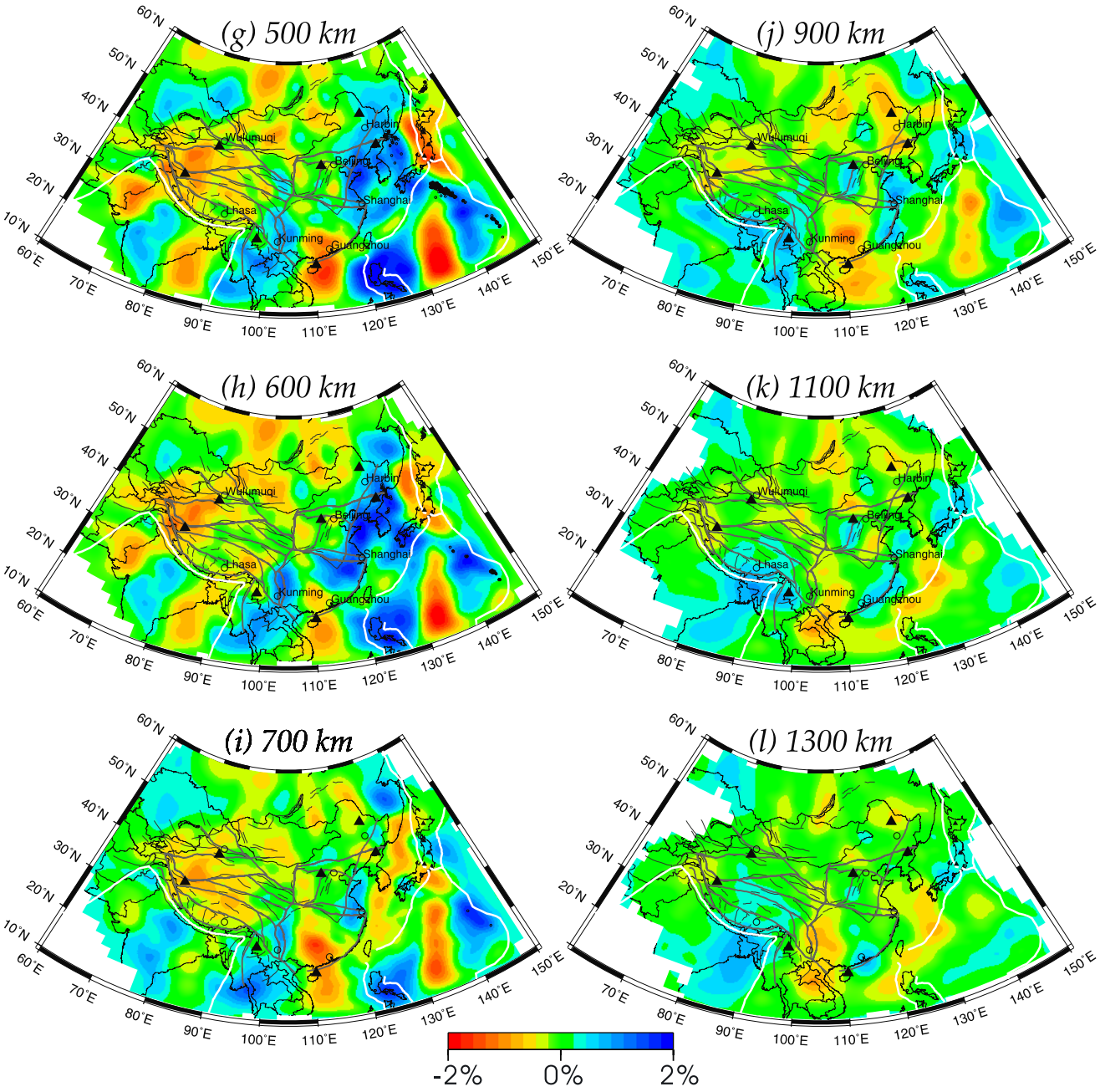

Figure 6. (continued)

performed several such tests by adopting different grid spacings. Figure 5 shows the results of a checkerboard resolution test with a grid spacing of 2°. At the depth of 15 km, the resolution is good in the Japan Islands and mainland China where many stations and earthquakes are located, but the surrounding regions have a lower resolution, which is expected. From 50 to 900 km depth, the resolution is good for most of the study region. At depth of 900 km, the central part of the study area still has good resolution. The addition of PP and pP rays helped to improve the resolution of the upper mantle. Although PcP rays are used, its number is limited, so the lower mantle below 1100 km has a low resolution. Our checkerboard tests with smaller grid spacings show that the spatial resolution is 100–150 km for the upper mantle and 150–200 km in the lower mantle down to about 1100 km depth. Hence, in the following, we will mainly discuss the structures down to 1100 km depth.

4. Results

4.1. Plan Views

[11] Figure 6 shows plan views of the P wave velocity images obtained. Plate boundaries, large fault zones, tectonic lines, background seismicity and major volcanic centers are also shown in the velocity images. At depths of 15 to 300 km, the most significant features in eastern Asia are the high-velocity (high-V) anomalies corresponding to the

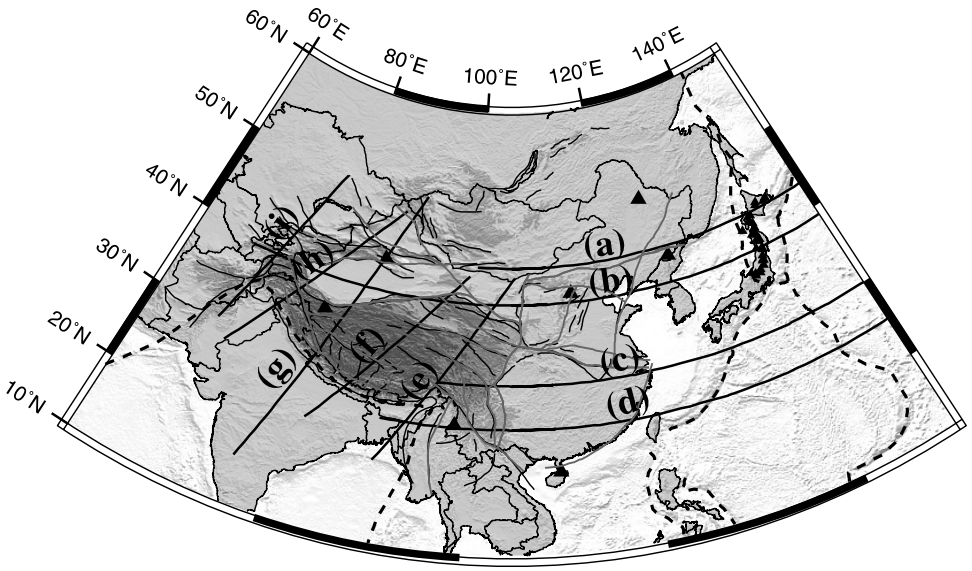

Figure 7. Map showing the locations of the vertical cross sections in Figure 8. Other labels are the same as those in Figure 1.

subducting Pacific and Philippine Sea slabs. The location of the high-V zones migrates gradually toward the west with the increasing depth, generally parallel with the oceanic trenches. We plotted the earthquakes relocated by *Engdahl et al.* [1998] in the velocity maps (Figure 6). It is clear that all the intermediate-depth and deep earthquakes are located in the high-V zones. Such a feature is clear particularly at layers of 50, 110 and 200 km depths. Under the Philippine Sea and between the subducting Pacific and Philippine Sea slabs, clear low-velocity (low-V) anomalies are visible from 15 to 900 km depth. At the crust and the shallow mantle the low-V zones may be associated with the Kyushu-Palau Ridge [*Seno et al.*, 1993]. In the deeper part of the upper mantle, the low-V zones may represent the hot mantle wedge under the Izu-Mariana arc and back arc, where fluids from the dehydration of the Pacific slab and corner flow in the mantle wedge result in magma and lead to the formation of active volcanoes in the Izu-Mariana arc and back arc, as well as back-arc spreading, similar to the structure and process under the Tonga arc and Lau back-arc basin [*D. Zhao et al.*, 1997].

[12] Under southwest China, high-V anomalies corresponding to the subducting Indian plate are visible down to about 300 km depth. The location of the slab moves gradually toward the north and its northern edge reaches to the Qiangtang block. Some high-V anomalies exist down to 1000 km depth or even deeper under south of the Himalaya arc, which might be pieces of the old Tethyan slab collapsing down to the lower mantle [*Van der Voo et al.*, 1999].

[13] In the depth range of 15 to 200 km, significant low-V anomalies exist under Japan Islands, marginal seas in western Pacific, and eastern China, and the low-V zones extend gradually toward the west with the increasing depth. Such wide extent of the low-V zones under east China is consistent with the suggestions about the thinning of the lithosphere under eastern China [e.g., *Zhao and Windley*, 1990; *Liu*, 1987; *Ren et al.*, 2002]. Under the intraplate volcanic areas such as Changbai, Datong and Tengchong, low-V zones exist from the surface down to 200–300 km depth. Under the Haikou volcanic area north of Hainan Island, a prominent low-V zone exists from the surface down to 1000 km or even deeper. This result is in good agreement with the recent global tomography results [*Zhao*, 2001, 2004], suggesting the existence of the Hainan plume originating from the lower mantle or core-mantle boundary (CMB).

[14] There are a number of sedimentary basins in China. The three large sedimentary basins in western China, Tarim, Jungger and Qaidam, exhibit low velocities in the velocity map at 15 km depth. Geological studies show that the three basins have sediments of over 10 km thick [*Metivier et al.*, 1999]. Under stable blocks such as Tarim basin, Sichuan basin, Junger basin and the Ordos block, high-V anomalies exist down to 200 km depth. Under the Tianshan orogenic belt, low-V anomalies are visible down to 110 km depth. These results suggest that these surficial features are associated with deep structure and processes in the upper mantle.

[15] At depths of 400–600 km, broad high-V anomalies are visible under eastern China, which show the images of the stagnant Pacific slab in the mantle transition zone [*Fukao et al.*, 2001; *Zhao*, 2001, 2004]. At 600 km depth, high-V zones exist in both the eastern and western parts of the Yangzi block. The eastern high-V zone is related to the Pacific slab, while the western high-V zone is associated with the Indian slab. At 700 km depth, the broad high-V anomalies disappear under eastern China, but still visible under Izu-Mariana. The interaction of the subducting slabs and the 660-km discontinuity will be discussed in section 5.1.

4.2. East-West Vertical Cross Sections

[16] Eight vertical cross sections along the profiles in Figure 7 are shown in Figure 8. Also shown in the cross sections are the surface topography, the locations of major

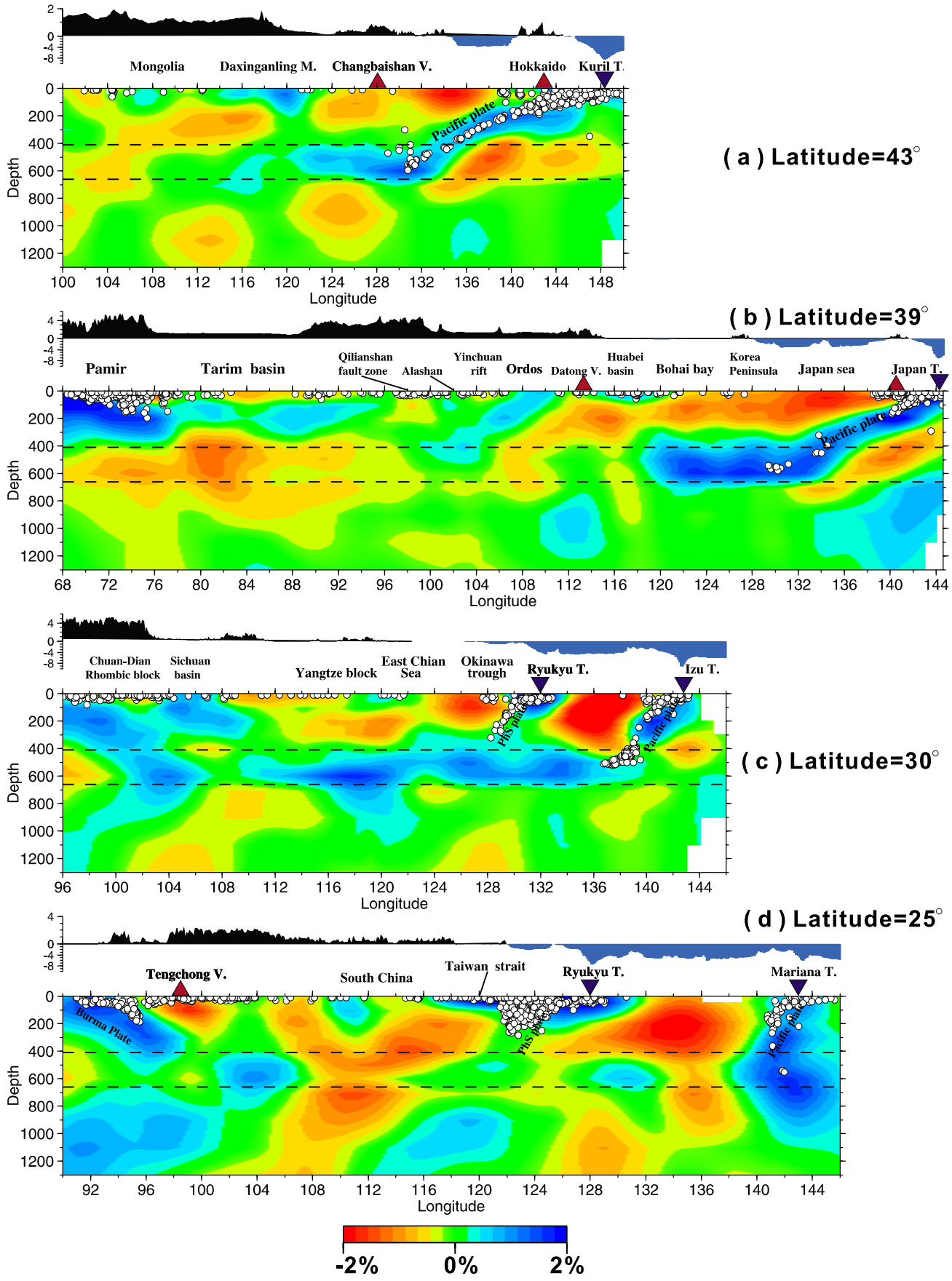
Mongolia
Daxinganling M.
Changbaishan V.
Hokkaido
Kuril T.
Pacific plate
Depth
Longitude
(a) Latitude=43°
Pamir
Tarim basin
Qilianshan fault zone
Alashan
Yinchuan rift
Ordos
Datong V.
Huabei basin
Bohai bay
Korea Peninsula
Japan sea
Japan T.
Pacific plate
(b) Latitude=39°
Chuan-Dian Rhombic block
Sichuan basin
Yangtze block
East Chian Sea
Okinawa trough
Ryukyu T.
Izu T.
PHS plate
Pacific Plate
(c) Latitude=30°
Tengchong V.
South China
Taiwan strait
Ryukyu T.
Mariana T.
Burma Plate
PHS Plate
Pacific Plate
(d) Latitude=25°
-2%
0%
2%

Figure 8

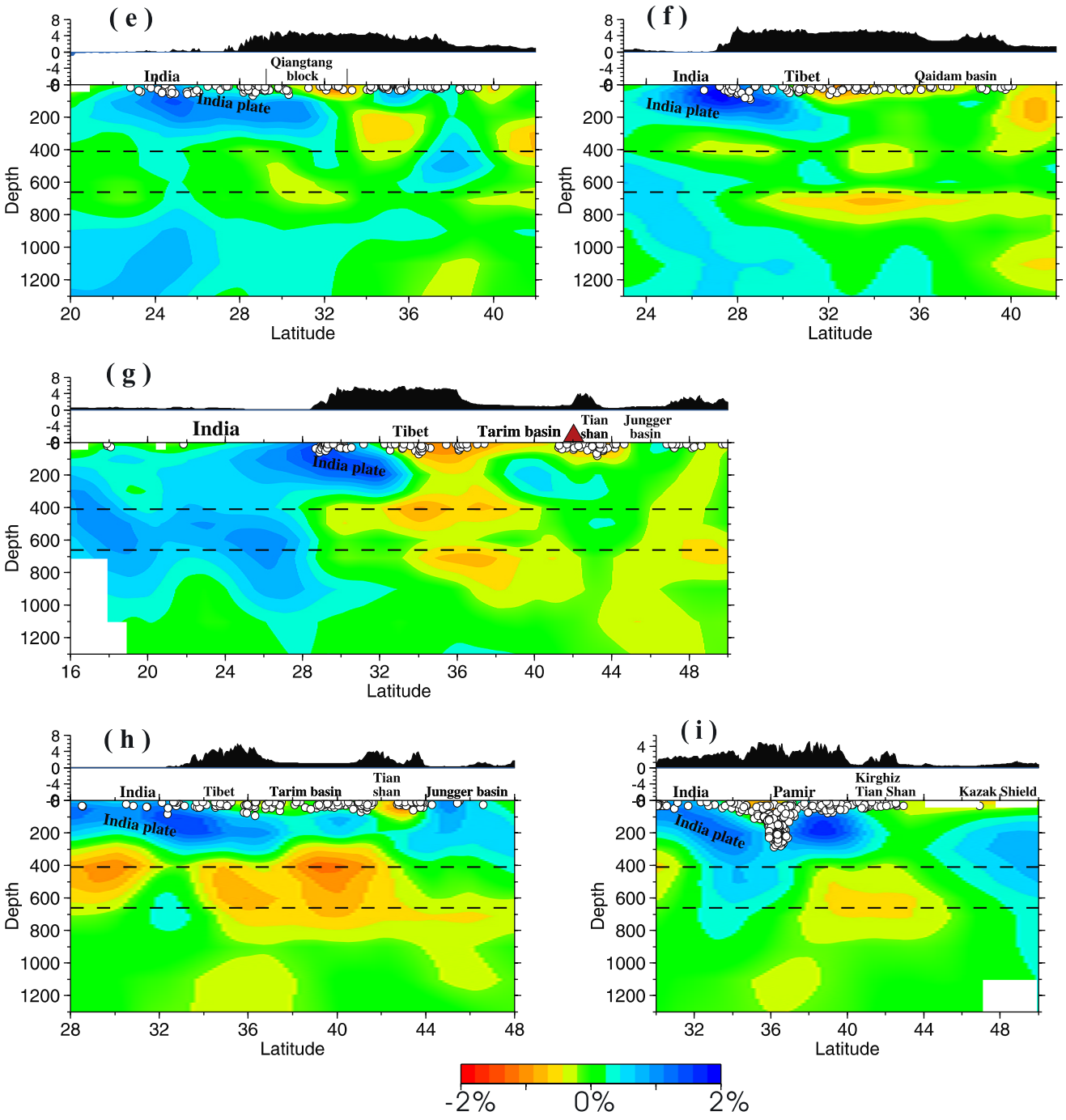

Figure 8. (continued)

tectonic units and earthquakes that occurred within 50 km of each profile. In the four E-W vertical cross sections (Figures 8a–8d), the most significant features are the high-V zones corresponding to the subducting Pacific and Philippine Sea slabs and low-V anomalies in the mantle wedge above the slabs.

[17] In Figure 8a, we can see that the Pacific slab subducts from the Kuril trench into the mantle with a moderate dip angle. At depths of 500–600 km, the slab suddenly becomes flat and stagnates in the mantle transition zone. The western edge of the stagnant slab reaches to 120°E longitude. The slab is located above the 660-km

Figure 8. Vertical cross sections of P wave velocity perturbations along the profiles shown in Figure 7. The surface and seafloor topography along each profile is shown on the top of each cross section. White dots show the earthquakes that occurred within a 50-km width from each profile. Red and blue triangles denote locations of volcanoes and oceanic trenches, respectively. The velocity perturbation scale is shown at the bottom. The dashed black lines denote the 410- and 660-km discontinuities.

discontinuity. The intermediate-depth and deep earthquakes form a clear Wadati-Benioff zone within the high-V slab. Prominent low-V zones exist in the mantle wedge down to about 200 km depth under the Japan arc and the Japan Sea, being generally consistent with the high-resolution local and regional tomography [*Zhao et al.*, 1992, 1994]. The mantle wedge low-V anomalies are also visible under the Changbai intraplate volcano down to about 300 km depth, being consistent with a recent local tomography of this region [*Zhao et al.*, 2004; *Lei and Zhao*, 2005]. However, the structure of the mantle transition zone had a lower resolution and the stagnant slab was not imaged well in the local tomography model [*Zhao et al.*, 2004; *Lei and Zhao*, 2005]. Our present model shows a much better image of the mantle wedge and the transition zone and reveals clearly the stagnant Pacific slab under the Changbai volcano. In the mantle under the subducting Pacific slab, some low-V anomalies are visible. This feature was also found in the previous regional and global tomgraphic images [*Zhao et al.*, 1994; *Zhao*, 2004].

[18] The cross section in Figure 8b passes through many important tectonic units in mainland China. Under the western edge of the cross section, a high-V zone is visible which corresponds to the low-angle descending Indian slab, and many shallow and intermediate-depth earthquakes occur along the upper slab boundary. This region is located in the western boundary of China and exhibits strong seismic activity. Under Tarim basin, a low-V zone exists down to about 15 km depth and a high-V zone extends down to 200–250 km depth, suggesting that the Tarim basin is located above a stable and thick craton. East of the Tarim basin, low-V anomalies exist under the Qilianshan fault zone, the Alashan block and the Yinchuan graben which are tectonically active regions with intensive seismic activity. The Ordos block is a stable region with low seismicity. A high-V zone exists under Ordos and dips toward the west down to about 300 km depth (Figure 8b). A recent local tomography also revealed high-V features in the upper mantle under Ordos [*Guo et al.*, 2004]. Under the Datong volcano in Shanxi graben, a prominent low-V zone exists down to about 400 km depth, and it is connected with low-V zones under the Huabei basin, Bohai bay, Korea Peninsula and Japan Sea, forming a big mantle wedge above the subducting and stagnant Pacific slab. The broad low-V zones may be related to the lithospheric thinning under eastern China. The subducting Pacific slab is clearly visible from the Japan Trench, and has a dip angle of about 28°. The western end of the stagnant slab reaches to approximately 119°E longitude.

[19] In Figure 8c the subducting Pacific slab has a dip angle of about 45° and extends down to 400 km depth. The slab becomes horizontal and stagnant in the mantle transition zone. The subducting Philippine Sea slab is also visible as a relatively high-V zone with intermediate-depth and deep earthquakes occurring down to about 300 km depth. The Philippine Sea slab is young and has a thickness of 30–40 km [*Zhao et al.*, 2000, 2002]; hence it is less well imaged as the Pacific slab due to the limited resolution scale of the present tomographic inversion. The stagnant slab in the transition zone looks thinner than that in Figures 8a and 8b, and part of the slab materials seems to extend below the 660-km discontinuity in the longitude range of 116 to 121°E. A strong low-V zone exists under the Okinawa trough down to about 200 km depth. Many previous studies have shown that this region exhibits high heat flow, active seismic and volcanic activities, and low velocity and high conductivity in the upper mantle [*Yamano et al.*, 1989; *Kaneko and Honura*, 1987; *Hao et al.*, 2004], and at the stage of active back-arc spreading [*Kimura*, 1985]. Under the Sichuan basin, a high-V zone exists down to a depth of 300 km (Figure 8c). Pn wave studies of the Sichuan basin show that seismic velocity is high in the uppermost mantle with little seismic anisotropy [*Hearn et al.*, 2004; *Liang et al.*, 2004; *J. Huang et al.*, 2003]. The seismicity is very low, and there are no large earthquakes in this region. These results suggest that the Sichuan basin is a tectonically stable region. Under the western edge of the cross section (Figure 8c), a high-V zone dips toward the east and exists in the upper mantle and the mantle transition zone, which may show the subducting Indian slab. This region is located in the northeastern end of the Burma arc where the Indian plate is subducting toward the north while the Burma microplate descends toward the east under the Eurasian plate. Hence this region has very complex structure and tectonics with intensive seismic and volcanic activities.

[20] The cross section in Figure 8d passes through the active Tengchong volcano in southwest China. A high-resolution local tomography revealed low-V anomalies in the crust and upper mantle down to 85 km depth under the volcano [*Huang et al.*, 2002]. However, the deeper structure was unknown because the local tomography model was limited to 85 km depth. Our present result shows low-V zones extending down to 300 km depth under the Tengchong volcano and a dipping high-V zone corresponding to the subducting Burma microplate with intermediate-depth earthquakes within it down to about 200 km depth (Figure 8d). This result indicates that the origin of the Tengchong volcano is closely related to the subduction of the Burma microplate. The high-V zone corresponding to the subducting Pacific slab extends down to about 1000 km under the Bonin arc, and there is no stagnant slab in the transition zone (Figure 8d). The Wadati-Benioff deep seismic zone is nearly vertical. These results indicate that the subducting Pacific slab has penetrated the 660-km discontinuity and reached to the lower mantle under the Bonin arc. The high-V zone corresponding to the descending Philippine Sea slab and the intermediate-depth earthquakes within it extend down to about 300 km depth.

4.3. Vertical Cross Sections Under Southwest China

[21] Figures 8e–8i show five vertical cross sections of tomographic images passing though the Tibetan Plateau. We can see that the Indian plate is imaged clearly as high-V zones, which is subducting beneath the Tibetan Plateau down to a depth of 200 to 300 km with low angle. The horizontal distance of the subduction Indian slab is about 500 km, and the northern edge of the slab reaches to the Qiangtang block (Figure 8e). Broad high-V anomalies are also visible in the mantle transition zone and lower mantle (Figures 8e, 8f, and 8g), which may represent the late Mesozoic Tethyan slabs subducted before the India-Asia collision [*Van der Voo et al.*, 1999].

[22] Relatively high velocity bodies exist in the lower crust and upper mantle under the Tarim basin (Figures 8g

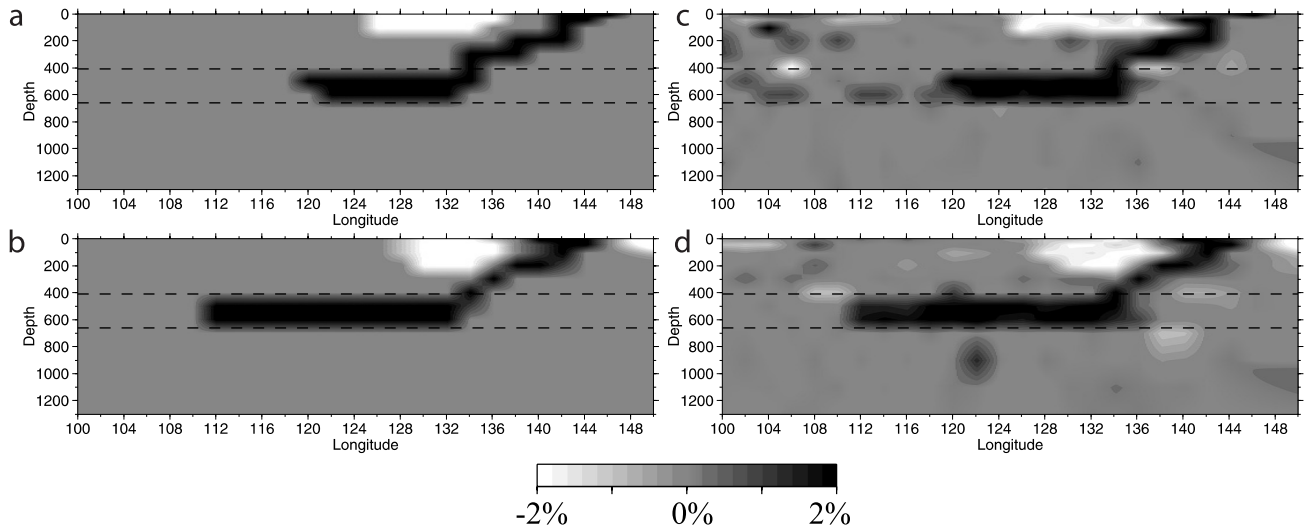

Figure 9. Results of synthetic tests along (a, c) 30°N and (b, d) 40°N latitudes. Input models (Figures 9a and 9b) and recovered results (Figures 9c and 9d). The velocity perturbation scale is shown at the bottom.

and 8h), Qaidam basin (Figure 8f) and Jungger basin (Figure 8h), which were also revealed by a previous regional tomographic imaging [*Xu et al.*, 2002]. These results suggest that these basins are pieces of old rigid lithospheric blocks and they have kept their general shapes even after many tectonic movements in the long geological history. Figure 8h shows that the descending Indian slab under the western Himalaya arc has reached to the southern margin of the Tarim basin, and the high-V Indian slab has nearly contacted the high-V body under the basin. This feature is well consistent with the deep seismic sounding results using artificial explosions [*Gao et al.*, 2000].

[23] The Tianshan orogenic belt exhibits lithospheric structure very different from the adjacent basins (Figure 8h). A low-V zone exists down to about 100 km depth under Tianshan, while the high-V zone under the Tarim basin extends into the asthenosphere under Tianshan. The vertical uplifting rate amounts to 1.7 cm/yr in Tianshan [*Peng*, 1993]. GPS surveys [*Wang and Ding*, 2000] showed that the convergent rate is 0.4 cm/yr in eastern Tianshan (87°E) and 2 cm/yr (fast shortening) in western Tianshan (76°E) which is nearly a half of the convergent rate between the Indian and Eurasian plates. Large earthquakes occur frequently in the Tianshan and Pamir region, being seismically the most active region in central Asia. Geological investigations show that Tianshan has very complex geological structures with various types of rocks because of the frequent and complicated tectonic movements with large-scale volcanic eruptions in the long geological history [*Deng et al.*, 2000]. The intensive seismic activity and large crustal deformation in the Tianshan orogenic belt may be related to the complex structure and tectonics in the upper mantle under this region. So far many researchers have investigated the deep structure and dynamic processes of the Tianshan orogenic belt [e.g., *Cotton and Avouac*, 1994; *Kosarev et al.*, 1993; *Roecker et al.*, 1993; *Chen et al.*, 1997; *Ghose et al.*, 1998]. *Vinnik and Saipekova* [1984] suggested that a mantle upwelling exists under western Tianshan and the elevation of the Tianshan mountains is related to a small-scale mantle convection. This hypothesis has been supported by body wave and surface wave tomographic studies and the investigation of seismic anisotropy with shear wave splittings [*Roecker et al.*, 1993; *Curtis and Woodhouse*, 1997; *Kosarev et al.*, 1993; *Makeyava et al.*, 1992; *Xu et al.*, 2002]. Our present result is also consistent with these previous studies.

[24] Pamir is located at the northwestern edge of the India-Asia collision zone, and is the seismically most active region in the western boundary area of China. It is also an unusual continental area in the world with active intermediate-depth seismicity, and so it has been paid much attention by many seismologists. There are different views on the tectonic background for the occurrence of the intermediate-depth earthquakes [e.g., *Molnar and Tapponnier*, 1975; *Billington et al.*, 1977; *Roecker et al.*, 1980; *Ning and Zang*, 1990]. The cross section in Figure 8i passes through the Pamir region, which shows that the subducting Indian slab (high-V zone) is colliding with the rigid Tajik and Tarim blocks (high-V zone) and forms a V-shape structure between them. The intermediate-depth earthquakes occur actively in and around the V-shape area, suggesting that these earthquakes are caused by the colliding process between the two rigid blocks. On the surface the collision leads to the formation of arc-like mountainous structures toward the north in the Pamir region, while the tectonic stress at depth is released in the form of intermediate-depth earthquakes. Focal mechanism solutions of the shallow and deep earthquakes also indicate that the modern tectonic stress originates from the India-Asia collision in the north-south direction [*Ning and Zang*, 1990].

4.4. Restoring Tests for the Stagnant Slab

[25] Our results show clearly that the Pacific slab becomes stagnant in the mantle transition zone under NE Asia (Figures 8a–8c). To confirm this feature, we conducted several restoring tests. The synthetic model adopted for the restoring tests contains the high-V stagnant slab in the mantle transition zone with different lengths along different latitudes and low-V anomalies in the mantle wedge above the slab (Figures 9a and 9b), which are

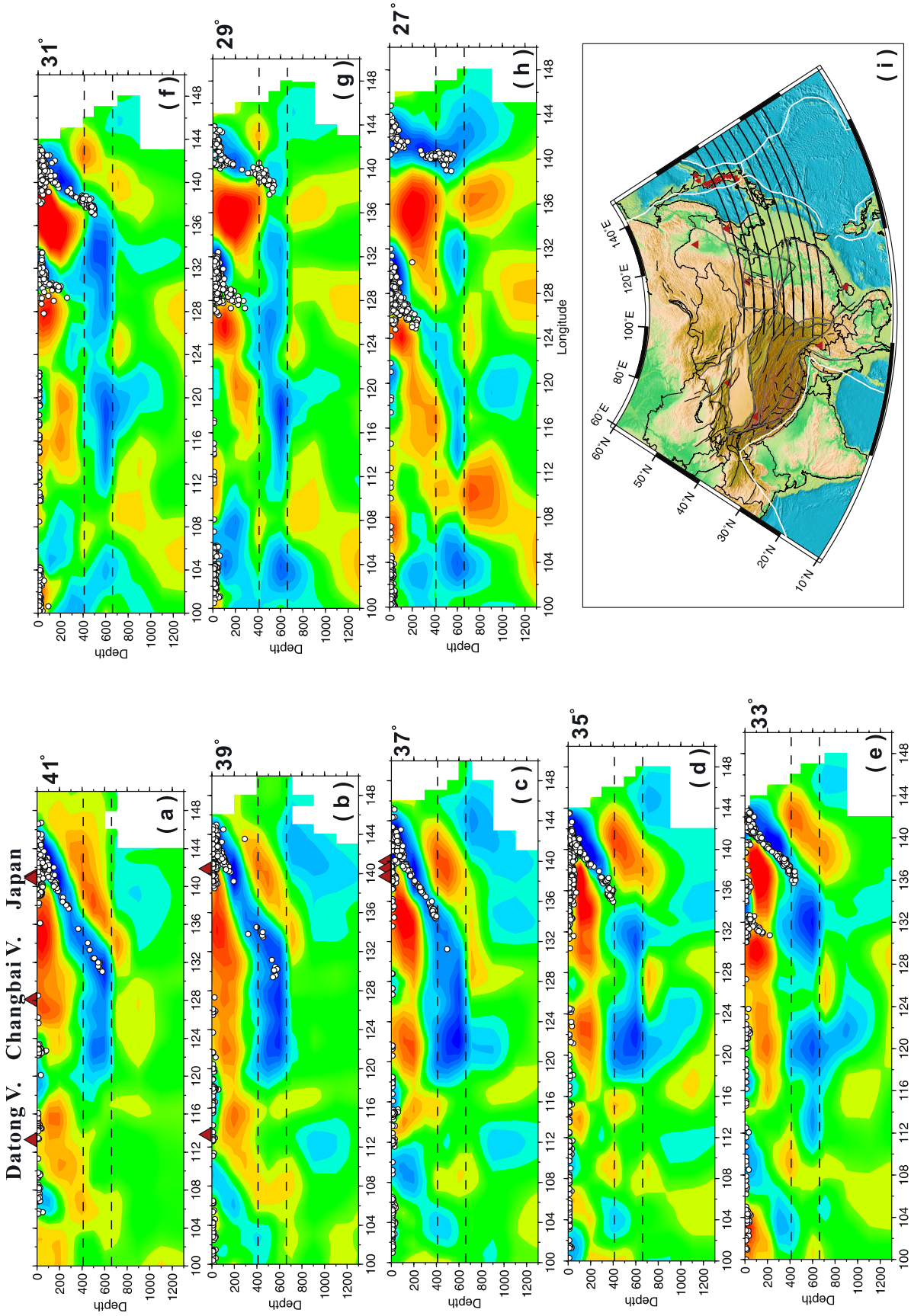
Datong V.
Changbai V.
Japan
41°
39°
37°
35°
33°
31°
29°
27°
(a)
(b)
(c)
(d)
(e)
(f)
(g)
(h)
(i)
Depth
Longitude
%
-2
-1
0
1
2
60°N
50°N
40°N
30°N
20°N
10°N
60°E
80°E
100°E
120°E
140°E

Figure 10

derived from our inversion results (Figures 8a–8c). The results of these restoring tests show that these features are nicely recovered after the inversion of the synthetic data (Figures 9c and 9d). Therefore we believe that the stagnant Pacific slab in the transition zone under east Asia can be imaged reliably with our data set and inversion technique, and so it is a very reliable feature.

5. Discussion

5.1. Effect of the Subducting Pacific Slab on East Asian Tectonics

[26] In the eastern portion of the present study region, the Pacific plate is subducting beneath the Eurasian plate from Kuril trench, Japan trench, Izu-Bonin trench and Mariana trench, forming the largest trench–arc–back-arc system on Earth. So far, many regional and global tomographic studies have been made to investigate the 3-D mantle structure of the western Pacific subduction zone, and have revealed the general structure of the subducting slab [e.g., *Zhou and Clayton*, 1990; *Zhao et al.*, 1994; *Bijwaard et al.*, 1998; *Fukao et al.*, 2001; *Zhao*, 2001, 2004]. Compared with these previous studies, we have used a much better data set and obtained much clearer images of the subducting Pacific slab under NE Asia. In this section, we discuss the morphology of the Pacific slab in the mantle transition zone and the influence of the subducting Pacific slab on east Asian tectonics.

[27] Figure 10 shows eight E-W vertical cross sections passing through east Asia. The separation of the cross sections is 2° in the latitude direction. From the oceanic trench to about 400 km depth, the dipping angle of the Pacific slab changes systematically. Under the Kuril arc the slab is steep with a dipping angle of 40° to 31°. Under the Japan arc the slab dipping angle becomes gradually smaller from the north to south, from 31° to 28°. From the Japan arc to the Izu-Mariana arc, the slab becomes steep again. The slab dipping angle is 31° at 35°N latitude and becomes 50° at 31°N latitude, and is nearly 90° at 27°N latitude. The high-V zone corresponding to the slab even rolls back toward the trench side in the range of 27 to 25°N latitude. The geometry of the Wadati-Benioff deep seismic zone is well consistent with the morphology of the high-V zone in each of the cross sections (Figure 10). The shape of slabs under Kuril, Izu-Bonin and Mariana obtained by this study is similar to the results from globe tomography [e.g., *Bijwaard et al.*, 1998; *Zhao*, 2004].

[28] It is generally considered that the dip of the subducting slab and the degree of interplate seismic coupling depend on many factors, but particularly on the age and convergent rate of the oceanic plate before subduction [*Uyeda and Kanamori*, 1979; *Ruff and Kanamori*, 1980; *Zang and Ning*, 1996]. Older and slower subducting slabs usually have larger dipping angles. The subduction rate of the Pacific plate is 9–10 cm/yr at the Japan trench, 8–9 cm/yr at the Kuril trench, and 4.5–5.8 cm/yr at the Izu-Bonin trench [*Zang and Ning*, 1996]. This trend is generally consistent with the slab images we determined (Figure 10).

[29] In Figure 11 we compare the surface topography of China and surrounding regions with the tomographic image at 600 km depth. In east China, the surface topography changes suddenly from east to west, the boundary is oriented NNE to SSW, generally parallel with the Japan trench and the Ryukyu trench (Figure 11a). The topographic boundary also corresponds to a sudden change in the gravity field in east China. The stagnant Pacific slab is clearly visible in the tomographic image at 600 km depth (Figure 11b). The western edge of the stagnant slab (the red curved line in Figure 11b) is generally parallel with the Japan trench and the Ryukyu trench and roughly coincides with the boundary of the big surface topographic change (blue line in Figure 11b). Note that there are some discrepancies between the topographic boundary and the western edge of the stagnant slab, but both of them are located approximately 1800 km west of the trenches. This correlation may indicate that the subduction of the Pacific slab and its stagnancy in the mantle transition zone under east Asia have a great influence on the structure and tectonics of the crust and upper mantle under east China. The upper mantle above the stagnant slab may form a big mantle wedge [*Zhao et al.*, 2004; *Lei and Zhao*, 2005]. Corner flow in the big mantle wedge and deep slab dehydration may cause the upwelling of the hot asthenospheric materials, resulting in the thinning and fracture of the lithosphere under east China. The formation of the surface topography and gravity anomaly boundary, the great Tanlu fault zone, strong intraplate earthquakes, active intraplate volcanism, and the abundant oil and other natural mineral resources in east China may be all related to this deep structure and dynamic processes.

[30] It has been long debated whether the subducting slab can penetrate into the lower mantle. Although receiver function studies suggest that part of the slab materials have penetrated into the lower mantle under NE China [e.g., *Ai et al.*, 2003; *Li and Yuan*, 2003], our present tomographic images show that all the present slab materials are stagnant in the mantle transition zone (Figures 10a and 10b) under NE China. South of 37°N latitude, however, some of the slab materials are visible below the 660-km discontinuity, while most of the slab materials are still in the transition zone (Figures 10c–10g). In the region south of 27°N latitude, the Pacific slab penetrates directly into the lower mantle. Such a pattern of slab's behavior is also visible in the tomographic image at 700 km depth in Figure 6. The subducting Philippine Sea slab may have also reached to the mantle transition zone and become stagnant there together with the Pacific slab (Figures 10f–10h). Recent global tomography studies revealed high-V anomalies in the lower mantle down to the CMB under east Asia, suggesting that after a long time stagnancy in the mantle transition zone, the slab materials can finally collapse down to the bottom of the mantle as a result of gravitational instability from phase transitions [e.g., *Zhao*, 2004].

Figure 10. (a–h) East-west vertical cross sections of P wave velocity perturbations along the profiles shown in (i) the map. The latitude of each cross section is shown on the right. Red and blue colors denote low and high velocities, respectively. The velocity perturbation scale is shown at the bottom. Other labels are the same as those in Figure 8.

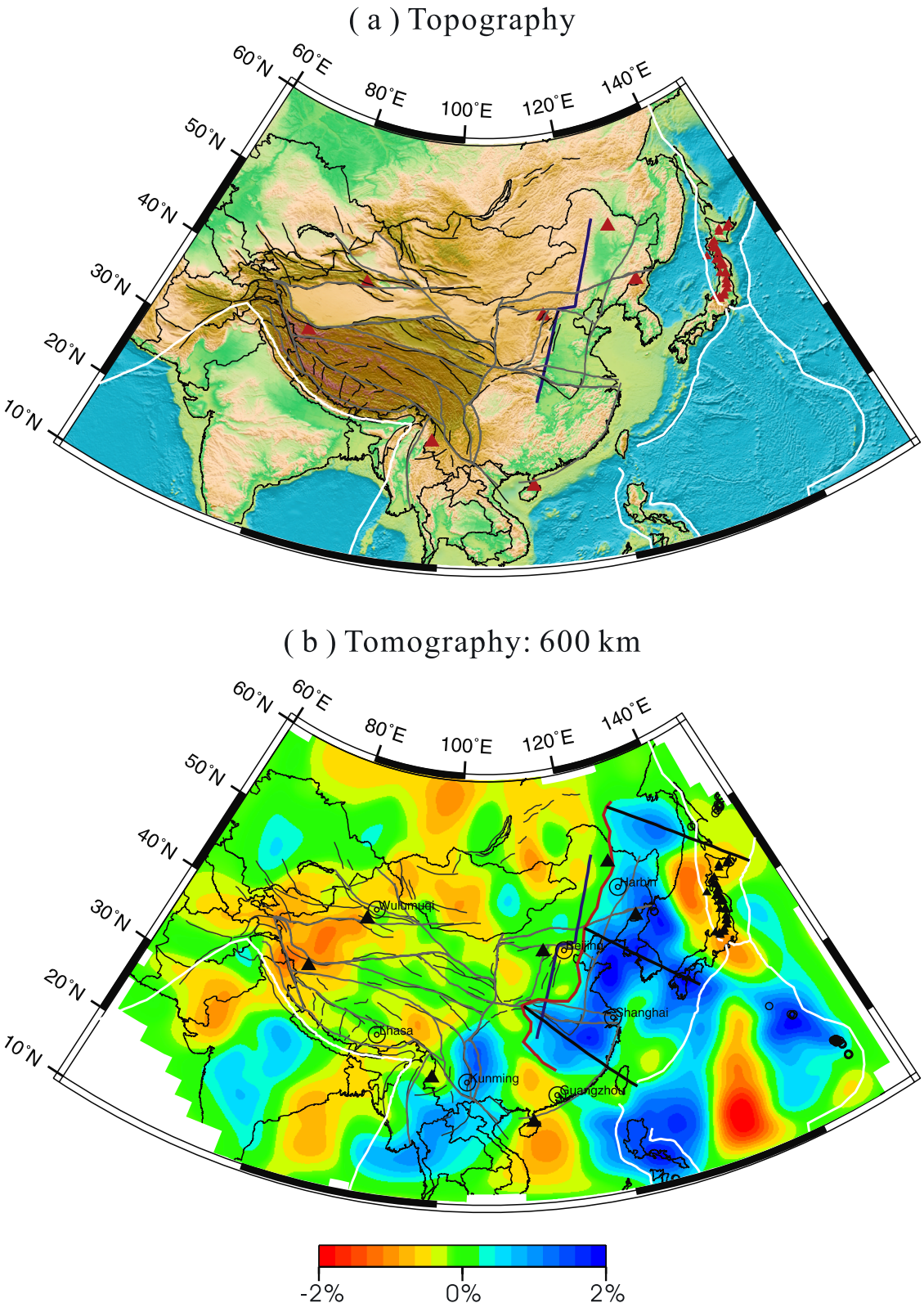

Figure 11. (a) Surface topography of the study region and (b) tomographic image at 600 km depth. The blue lines denote the topographic boundary, and the red curved lines denote the western edge of the stagnant slab in the mantle transition zone.

5.2. India-Asia Collision and Subduction

[31] The India-Asia collision and the subduction of the Indian plate under the Tibetan Plateau have long attracted geoscientists in the world and have been investigated with various geological and geophysical approaches [e.g., *Yin and Harrison*, 2000; *Tapponnier et al.*, 1986; *Allegre et al.*, 1984; *Zhao et al.*, 1993; *Molnar et al.*, 1987; *Nelson et al.*, 1996]. Early studies proposed many different models of the India-Asia collision and subduction [e.g., *Powell*, 1986; *Beghoul et al.*, 1993; *Willett et al.*, 1993]. On the basis of the detailed seismological results of the crust and upper mantle structure under Tibet [*W. Zhao et al.*, 1997], *Zeng et al.* [2000] proposal a model suggesting the subduction of multilayer Indian crust and the crust-mantle delamination. This model seems to have been supported by receiver function and global tomographic studies [*Kind et al.*, 1996; *Zhang and Tanimoto*, 1993; *Su et al.*, 1994; *Zhou*, 1996]. *Zeng et al.* [2000] suggested that during the subduction under the Tibetan plateau the Indian plate is divided into the upper crust and the upper mantle lid. The plastic lower crust makes it possible for the upper mantle lid to detach the upper crust. During the process of the advancing of the upper crust at different periods, multilayer crust subduction took place under the Himalaya and southern Tibet [*W. Zhao et al.*, 1997], while at the same time the upper mantle lid was subducting to the deeper part of the upper mantle [*Zhang and Tanimoto*, 1993; *Su et al.*, 1994; *Kind et al.*, 1996; *Zhou*, 1996]. This style of subduction is quite different from that of the oceanic plate subduction.

[32] Our present 3-D velocity model of China has a much higher spatial resolution than that of the global tomographic models [*Zhang and Tanimoto*, 1993; *Su et al.*, 1994; *Zhou*, 1996; *Zhao*, 2001]. Although our model still cannot image the multisubduction in the crust, it clearly shows the existence of low-V anomalies in the lower crust (Figure 6). Our tomographic images clearly show that the Indian plate is subducting under the Tibet at a low angle down to 200–300 km depth (Figures 8e–8i). The northern edge of the subducting Indian plate has reached to the Qiangtang block. The horizontal distance of the subduction is 500–700 km. Our present results provide further evidence supporting the delamination model of *Zeng et al.* [2000].

5.3. Origin of the Intraplate Volcanoes in China

[33] Several active intraplate volcanoes exist in mainland China, e.g., the Wudalianchi and Changbai volcanoes in NE China and Tengchong volcano in SW China (see the map in Figures 1, 6, and 7). The Wudalianchi volcano in northern Heilongjiang Province erupted in A.D. 1719 and 1721. The Changbai volcano that is located at the border between Chinese Jilin Province and North Korea erupted in A.D. 1050, 1120, 1193, and 1410. The origin of these volcanoes is still unclear. Some researchers consider them to be hot spots [e.g., *Turcotte and Shubert*, 1982], while others invoked the asthenospheric injection to explain them [*Tatsumi et al.*, 1990]. Our tomographic images show that very slow anomalies exist in the upper mantle right beneath the Wudalianchi and Changbai volcanoes, right above the stagnant Pacific slab in the mantle transition zone (Figures 10a). This result is quite similar to the images under the Fiji-Tonga region where the back-arc volcanoes in Fiji and the Lau spreading center are located above very slow anomalies in the mantle wedge right above the subducting Tonga slab [*D. Zhao et al.*, 1997]. These results suggest that the active volcanoes in northeast China are not hot spots but a sort of back-arc volcanoes which are closely related to the subduction process of the Pacific slab [*Zhao*, 2004; *Zhao et al.*, 2004]. Slow velocity anomalies in the back-arc region are generally associated with the back-arc magmatism and volcanism caused by the deep dehydration process of the subducting slab and the convective circulation process of the mantle wedge [*D. Zhao et al.*, 1994, 1997, 2002]. These processes lead to the large-scale upwelling of the asthenospheric materials under northeast China and cause intraplate volcanism and continental rift systems in the region. *Tatsumi et al.* [1990] first proposed the asthenospheric injection to explain the formation of the Wudalianchi and Changbai volcanoes, but they did not consider the stagnant Pacific slab under the region because such a slab structure was unknown at that time. Here we emphasize the role of the stagnant Pacific slab in the formation of the intraplate volcanism in east Asia.

[34] The Tengchong volcano is a prominent active volcano in SW China. Its last eruption was in 1609. In recent years many volcanic tremors have occurred in the region, indicating the magmatic activity under the volcano and the potential of future eruptions. From its proximity to the plate boundary, active local seismicity and focal mechanism solutions, some researchers suggested that the origin of the Tengchong volcano was related to the India-Asia collision [*Huangfu and Jiang*, 2000]. However, until now there has been no definite structural evidence for that. A high-resolution local tomography revealed low-V anomalies in the crust and upper mantle down to a depth of 85 km under the volcano [*Huang et al.*, 2002]. Seismic explosion studies also showed the existence of low-V anomalies in the crust [*Wang et al.*, 2002]. However, these studies could not resolve the depth extension of the low-V zone under the volcano. Global tomographic studies could not detect any clear low-V or high-V anomalies in the mantle under the Tengchong volcano due to the lower resolution. Our present results, however, show clearly a prominent low-V zone under the Tengchong volcano down to 300 km depth and the subducting Burma microplate (high-V) under the volcano down to about 400 km depth (Figure 8d). No other low-V anomalies are visible in the mantle transition zone and the lower mantle under the Tengchong region. These results indicate that the Tengchong volcano is not a hot spot associated with a deep mantle plume, it is more likely to be caused by the eastward subduction of the Burma microplate. Although the detailed process is still unclear, the subduction of the Burma microplate may cause corner flow in the wedge portion above the slab, and slab dehydration may take place. Similar to the arc volcanism associated with the oceanic plate subduction, these processes may lead to the formation of magma chambers in the mantle wedge, resulting in the Tengchong volcano. Recent petrological and geochemical studies show that the Tengchong volcanics have origin in the upper mantle [*Du et al.*, 2005], in support of our tomographic result.

5.4. Three Stable Blocks in China

[35] In the Chinese continent, there are three regions which are tectonically relatively stable compared with the

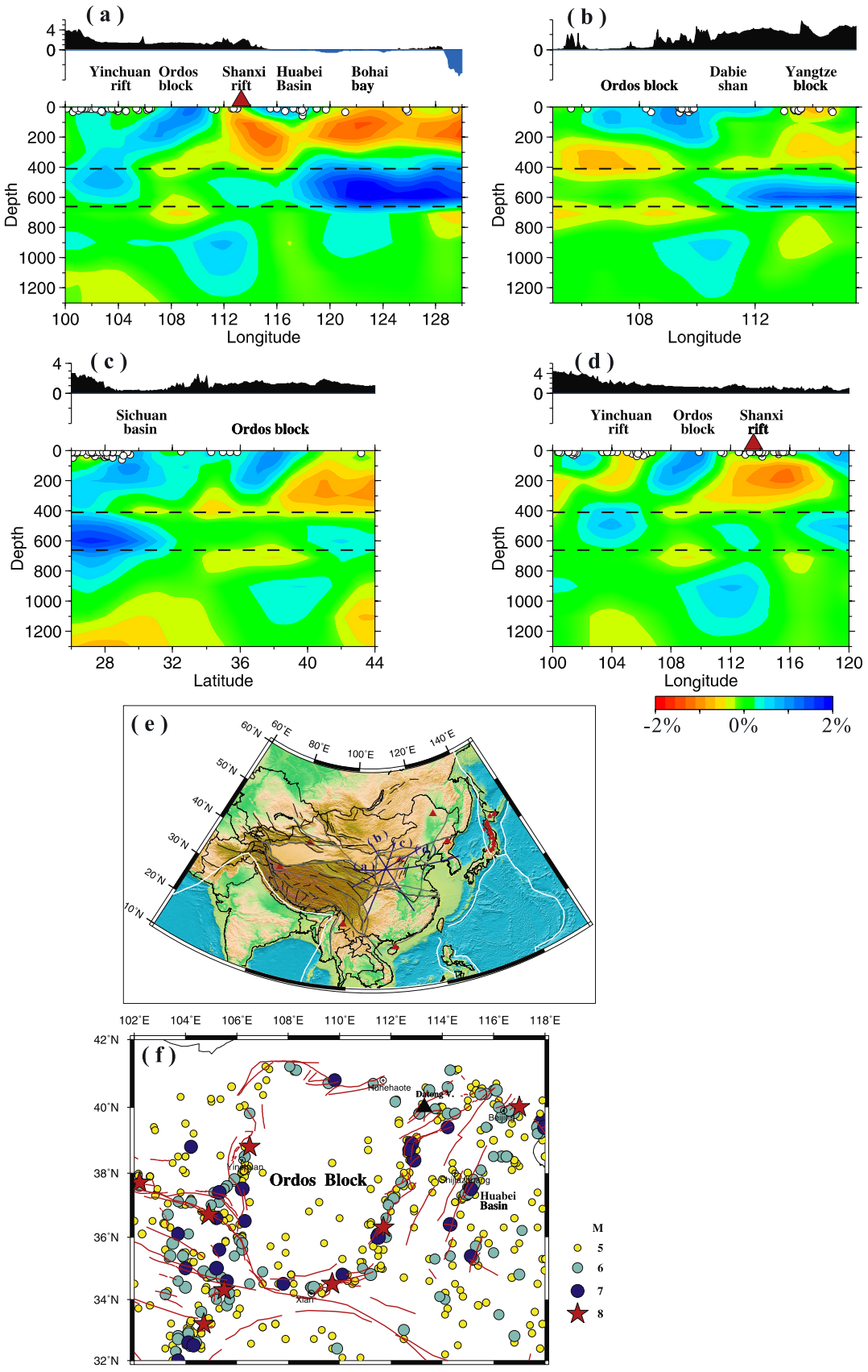

Figure 12. (a–d) Vertical cross sections passing through the Ordos block along the profiles shown in (e) the map. Other labels are the same as those in Figure 8. (f) Distribution of earthquakes and active faults (red solid lines) in and around the Ordos block. The earthquake magnitude scale is shown on the right. The black triangle denotes the Datong Quaternary volcano.

surrounding areas. They are the Tarim basin, Ordos block and Sichuan basin. The Tarim block contains Paleozoic rocks and is the oldest region in western China. Our tomographic results show that it has the thickest sedimentary layer among all the basins in China and that high-V anomalies under Tarim extends down to 300 km depth, which is generally consistent with the regional tomographic result [*Xu et al.*, 2002].

[36] The Ordos block is a distinct region in northern China. It is surrounded by active fault zones (Figure 12f). Many large earthquakes occurred outside of Ordos, while few occurred inside of it. In our tomographic images (Figures 12a–12d) the Ordos block shows up as a high-V zone which dips toward southwest and extends down to about 300 km depth, and it is surrounded by low-V anomalies in the crust and upper mantle. High-V anomalies also exist under the Sichuan basin and extend down to about 300 km depth (Figures 6 and 8c). Under the three stable blocks, Pn velocity is higher with weaker seismic anisotropy in the uppermost mantle than the surrounding region, which is considered to be consistent with the low seismicity and stable tectonic features there [*Hearn et al.*, 2004; *Liang et al.*, 2004].

[37] The three stable blocks may be composed of rigid rocks and so have been less deformed under the compressional stress regime caused by the westward subduction of the Pacific and Philippine Sea plates and the India-Asia collision from the southwest direction. They may have played an important role in the formation and tectonic evolution of the Chinese continent.

6. Conclusions

[38] Main findings of the present work can be summarized as follows.

[39] The subducting Pacific slab is imaged clearly as a high-velocity zone from the oceanic trenches down to about 600 km depth, and intermediate-depth and deep earthquakes are located within the slab. The Pacific slab becomes stagnant in the mantle transition zone under eastern China. The western edge of the stagnant slab is generally parallel with the Japan trench and the Ryukyu trench and roughly coincides with the boundary of a big surface topographic change. Although there are some discrepancies between the topographic boundary and the western edge of the stagnant slab, both of them are located approximately 1800 km west of the trenches.

[40] All Pacific slab materials are stagnant in the mantle transition zone under NE China (53°∼37° N latitudes). Under 37°∼28° N latitudes, however, some of the slab materials are visible below the 660-km discontinuity, though most of the slab materials are still in the transition zone. Under the Mariana arc, the Pacific slab penetrates directly down to the lower mantle.

[41] The subducting Indian and Philippine Sea plates are imaged clearly. The Indian plate has subducted down to 200–300 km depth under the Tibetan plateau with a horizontal subduction distance of about 500 km.

[42] There are three active intraplate volcanoes in China. The Changbai and Wudalianchi volcanoes in northeast China are underlain by significant slow anomalies in the upper mantle, above the Pacific stagnant slab, suggesting that the two active volcanoes are not hot spots but a kind of back-arc volcanoes associated with the deep subduction of the Pacific slab and its stagnancy in the transition zone. The active Tengchong volcano in southwest China is related to the eastward subduction of the Burma microplate.

[43] There are three tectonically stable regions in China: the Tarim basin, Ordos block, and the Sichuan basin. High-velocity anomalies are revealed in the upper mantle under the three regions, suggesting that they are composed of rigid rocks and so have been less deformed in the long geological history. The three stable blocks may have played an important role in the formation and tectonic evolution of the Chinese continent.

[44] **Acknowledgments.** We thank the Center of Chinese National Seismic Network for providing a part of the data used in this study. D. Wei provided the digital data for the geographic locations of the plate boundaries [*Wei and Seno*, 1998]. Two anonymous referees and the Associate Editor provided valuable review comments which improved the manuscript. This work was partially supported by National Development and Reform Commission of China (grant 2004-1138) and the Chinese Earthquake Study Foundation (103076) to J. Huang and grants from Japan Society for the Promotion of Science (Kiban-B 11440134 and Kiban-A 17204037) and a special grant for the Center of Excellence (COE) from Ehime University to D. Zhao. The figures are made by using GMT [*Wessel and Smith*, 1991].

References

Ai, Y., T. Zheng, W. Xu, Y. He, and D. Dong (2003), A complex 660 km discontinuity beneath northeast China, *Earth Planet. Sci. Lett.*, *212*, 63–71.

Allegre, C., V. Courtillot, and P. Tapponnier (1984), Structure and evolution of the Himalaya-Tibet orogenic belt, *Nature*, *307*, 17–22.

Beghoul, N., M. Baragang, and B. Isacks (1993), Lithospheric structure of Tibet and western North America: Mechanics of uplift and a comparative study, *J. Geophys. Res.*, *98*, 1997–2016.

Bijwaard, H., W. Spakman, and E. R. Engdahl (1998), Closing the gap between regional and global travel time tomography, *J. Geophys. Res.*, *103*, 30,055–30,078.

Billington, S., B. Isacks, and M. Barazagi (1977), Spatial distribution of focal mechanisms of mantle earthquakes in the Hindukush-Pamir region—A contorted Benioff zone, *Geology*, *5*, 699–704.

Chen, Y., S. Roecker, and G. Kosarev (1997), Elevation of the 410-km discontinuity beneath the central Tien Shan: Evidence for a detached lithospheric root, *Geophys. Res. Lett.*, *24*, 1531–1534.

Cotton, F., and P. Avouac (1994), Crust and upper-mantle structure under the Tian Shan from surface wave dispersion, *Phys. Earth Planet. Inter.*, *84*, 1–4.

Curtis, A., and J. Woodhouse (1997), Crust and upper mantle shear velocity structure beneath the Tibetan Plateau and surrounding regions from interevent surface wave phase velocity inversion, *J. Geophys. Res.*, *102*, 11,789–11,813.

Deng, Q., X. Feng, and P. Zhang (2000), *Active Tectonics of the Chinese Tianshan Mountains* (in Chinese), 399 pp., Seismol. Press, Beijing.

Du, J., C. Liu, B. Fu, Y. Ninomiya, Y. Zhang, C. Wang, H. Wang, and Z. Sun (2005), Variation of geothermometry and chemical-isotopic compositions of hot spring fluids in the Rehai geothermal field, southwestern China, *J. Volcanol. Geotherm. Res.*, *142*, 243–261.

Engdahl, E. R., R. D. van der Hilst, and R. Buland (1998), Global teleseismic earthquake relocation with improved travel times and procedures for depth determination, *Bull. Seismol. Soc. Am.*, *88*, 722–743.

Fukao, Y., S. Widiyantoro, and M. Obayashi (2001), Stagnant slabs in the upper and lower mantle transition region, *Rev. Geophys.*, *39*, 291–323.

Gao, R., D. Huang, and D. Lu (2000), Deep seismic reflection profile across the juncture zone between the Tarim basin and the west Kunlun mountains, *Chin. Sci. Bull.*, *45*, 2281–2286.

Ghose, S., W. Hamburger, and J. Virieux (1998), Three-dimensional velocity structure earthquake locations beneath the northern Tian Shan of Kyrgyzstan, central Asia, *J. Geophys. Res.*, *103*, 2725–2748.

Guo, B., Q. Liu, J. Chen, D. Zhao, S. Li, and Y. Lai (2004), Seismic tomographic imaging of the crust and upper mantle beneath the northeastern edge of the Qinghai-Xizang plateau and the Ordos area, *Chin. J. Geophys.*, *47*, 790–797.

Hao, T., J. Liu, F. Guo, Z. Huang, Y. Xu, M. Dai, A. Li, and Y. Fu (2004), Research on crustal structure and lithosphere property in the Okinawa trough area, *Chin. J. Geophys.*, *47*, 462–468.

Hearn, T. M., S. Wang, J. Ni, Z. Xu, Y. Yu, and X. Zhang (2004), Uppermost mantle velocities beneath China and surrounding regions, *J. Geophys. Res.*, *109*, B11301. doi:10.1029/2003JB002874.

Huang, J., and D. Zhao (2004), Crustal heterogeneity and seismotectonics of the region around Beijing, China, *Tectonophysics*, *385*, 159–180.

Huang, J., D. Zhao, and S. Zheng (2002), Lithospheric structure and its relationship to seismic and volcanic activity in southwest China, *J. Geophys. Res.*, *107*(B10), 2255, doi:10.1029/2000JB000137.

Huang, J., X. Song, and S. Wang (2003), Fine structure of Pn velocity beneath Sichuan-Yunnan region, *Sci. China, Ser. D*, *46*, suppl., 201–209.

Huang, Z., W. Su, Y. Peng, Y. Zheng, and H. Li (2003), Rayleigh wave tomography of China and adjacent regions, *J. Geophys. Res.*, *108*(B2), 2073, doi:10.1029/2001JB001696.

Huangfu, G., and C. Jiang (2000), *Investigation of the Tengchong Volcanic Activity* (in Chinese), 377 pp., Sci. and Tectnol. Publ. of Yunan Province, Kunming, China.

Kaneko, Y., and Y. Honura (1987), Electrical conductivity structure beneath the Okinawa Trough and the Ogasawara Arc, *Rep. Hydrogr. Res.*, *22*, 135–147.

Kennett, B. L. N., and E. R. Engdahl (1991), Traveltimes for global earthquake location and phase identification, *Geophys. J. Int.*, *105*, 429–465.

Kimura, M. (1985), Back-arc rifting in the Okinawa Trough, *Mar. Pet. Geol.*, *2*, 222–239.

Kind, R., J. Ni, W. Zhao, J. Wu, X. Yuan, L. Zhao, E. Sandvol, C. Reese, J. Nabelek, and T. Hearn (1996), Evidence from earthquake data for a partially molten crustal layer in southern Tibet, *Science*, *274*, 1692–1694.

Kosarev, G. L., N. V. Petersen, L. P. Vinnik, and S. W. Roecker (1993), Receiver functions for the Tien Shan analog broadband network: Contrasts in the evolution of structures across the Talasso-Fergana fault, *J. Geophys. Res.*, *98*, 4437–4448.

Lei, J., and D. Zhao (2005), P-wave tomography and origin of the Changbai intraplate volcano in northeast Asia, *Tectonophysics*, *397*, 281–295.

Leveque, J., L. Rivera, and G. Wittlinger (1993), On the use of the checkerboard test to assess the resolution of tomographic inversions, *Geophys. J. Int.*, *115*, 313–318.

Li, S., and W. D. Mooney (1998), Crustal structure of China from deep seismic sounding profiles, *Tectonophysics*, *288*, 105–113.

Li, X., and X. Yuan (2003), Receiver functions in northeast China–implicaplications for slab penetration into the lower mantle in northwest Pacific subduction zone, *Earth Planet. Sci. Lett.*, *216*, 679–691.

Liang, C., X. Song, and J. Huang (2004), Tomographic inversion of Pn travel times in China, *J. Geophys. Res.*, *109*, B11304, doi:10.1029/2003JB002789.

Liu, F., and A. Jin (1993), Seismic tomography of China, in *Seismic Tomography: Theory and Practice*, edited by H. M. Iyer and K. Hirahara, pp. 299–318, CRC Press, Boca Raton, Fla.

Liu, F., K. Qu, H. Wu, Q. Li, J. Liu, and G. Hu (1986), Seismic tomography of the north China region, *Chin. J. Geophys.*, *29*, 442–449.

Liu, F., H. Wu, J. Liu, G. Hu, Q. Li, and K. Qu (1990), 3-D velocity image beneath the Chinese continent and adjacent regions, *Geophys. J. Int.*, *101*, 379–394.

Liu, F., J. Liu, D. Zhong, J. He, and Q. You (2000), The subducted slab of Yangtze continental block beneath the Tethyan orogen on western Yunnan, *Chin. Sci. Bull.*, *45*, 466–471.

Liu, G. (1987), The Cenozoic rift system of the North China Plain and the deep internal process, *Tectonophysics*, *133*, 277–285.

Makeyava, L., L. Vinnik, and S. Roecker (1992), Shear-wave splitting and small convection in the continental upper mantle, *Nature*, *358*, 144–147.

Metivier, F., Y. Gaudemer, P. Tapponnier, and M. Klein (1999), Mass accumulation rates in Asia during the Cenozoic, *Geophys. J. Int.*, *137*, 280–318.

Molnar, P., and P. Tapponnier (1975), Cenozoic tectonics of Asia: Effects of a continental collision, *Science*, *189*, 419–426.

Molnar, P., P. England, and J. Martinod (1987), Mantle dynamics, the uplift of the Tibetan Plateau, and the Indian monsoon, *Rev. Geophys.*, *31*, 357–396.

Nelson, K., W. Zhao, and L. Brown (1996), Partially molten middle crust beneath southern Tibet: Synthesis of Project INDEPTH results, *Science*, *274*, 1684–1696.

Ning, J., and S. Zang (1990), The distribution of earthquakes and stress state in Pamir-Hindukush region, *Chin. J. Geophys.*, *33*, 657–669.

Paige, C. C., and M. A. Saunders (1982), LSQR, An algorithm for sparse linear equations and sparse linear system, *Trans. Math. Software*, *8*, 43–71.

Peng, S. (1993), On the Neotectonic movement in Tianshan reflected by the geodesic deformation survey (in Chinese), *Inland Earthquake*, *7*, 136–141.

Powell, C. (1986), Continental underplating model for the rise of the Tibetan, *Earth Planet. Sci. Lett.*, *81*, 79–94.

Ren, J., K. Tamaki, S. Li, and J. Zhang (2002), Late Mesozoic and Cenozoic rifting and its dynamic setting in eastern China and adjacent areas, *Tectonophysics*, *344*, 175–205.

Roecker, S., O. Soboleva, I. Nersesov, A. Lukk, D. Hatsfeld, J. Chatelain, and P. Molnar (1980), Seismicity and fault plane solutions and intermediate depth in the Pamir-Hinduhush region, *J. Geophys. Res.*, *85*, 1358–1364.

Roecker, S., M. Sabitova, P. Vinnik, A. Bormakov, I. Golvanov, and R. Mamatkanova (1993), Three-dimensional elastic wave velocity structure of the western and central Tian Shan, *J. Geophys. Res.*, *98*, 15,779–15,795.

Ruff, L., and H. Kanamori (1980), Seismicity and the subduction process, *Phys. Earth Planet. Inter.*, *23*, 240–252.

Seno, T., S. Stein, and A. Gripp (1993), A model for the motion of the Philippine Sea plate consistent with NUVEL-1 and geological data, *J. Geophys. Res.*, *98*, 17,941–17,948.

Su, W., R. Woodward, and A. Dziewonski (1994), Degree 12 model of shear velocity heterogeneity in the mantle, *J. Geophys. Res.*, *99*, 4945–4980.

Sun, R., and F. Liu (1995), Crust structure and strong earthquakes in Beijing, Tianjin and Tangshan area. I. P wave velocity structure, *Chin. J. Geophys.*, *38*, 599–607.

Tapponnier, P., G. Peltzer, and R. Armijo (1986), On the mechanics of the collision between India and Asia, in *Collision Tectonics*, edited by M. P. Coward and A. C. Ries, *Geol. Soc. Spec. Publ.*, *19*, 115–157.

Tatsumi, Y., S. Maruyama, and S. Nohda (1990), Mechanism of backarc opening in the Japan Sea: Role of asthenospheric injection, *Tectonophysics*, *181*, 299–306.

Turcotte, D., and G. Shubert (1982), Geodynamics, 450 pp., John Wiley, Hoboken, N. J.

Uyeda, S., and H. Kanamori (1979), Back-arc opening and the mode of subduction, *J. Geophys. Res.*, *84*, 1049–1061.

Van der Voo, R., W. Spakman, and H. Bijwaard (1999), Tethyan subducted slabs under India, *Earth Planet. Sci. Lett.*, *171*, 7–12.

Vinnik, L., and A. Saipekova (1984), Structure of lithosphere and asthenosphere of the Tien Shen, *Ann. Geophys.*, *2*, 621–626.

Wang, C., H. Lou, J. Wu, Z. Bai, G. Huangpu, and J. Qin (2002), Seismological study on the crustal structure of Tengchong volcano-geothermal area, *Acta Seismol. Sin.*, *24*, 231–242.

Wang, Q., and G. Ding (2000), Present-day crustal fast shortening in Tianshan and relative movement of the north-south blocks, *Chin. Sci. Bull.*, *45*, 1543–1547.

Wang, Q., P. Zhang, J. Freymueller, R. Bilham, and K. Larson (2001), Present-day crustal deformation in China constrained by global positioning system measurements, *Science*, *294*, 574–577.

Wei, D., and T. Seno (1998), Determination of the Amurian plate motion, in *Mantle Dynamics and Plate Interactions in East Asia*, *Geodyn. Ser.*, vol. 27, edited by M. Flower et al., pp. 337–346, AGU, Washington, D. C.

Wessel, P., and W. Smith (1991), Free software helps map and display data, *Eos Trans. AGU*, *72*, 441, 445–446.

Willett, S., C. Beaurront, and P. Fullsack (1993), Mechanical model for the tectonics of doubly vergent compression orogens, *Geology*, *21*, 371–374.

Xu, Y., F. Liu, J. Liu, and H. Chen (2002), Crust and upper mantle structure beneath western China from P wave travel time tomography, *J. Geophys. Res.*, *107*(B10), 2220, doi:10.1029/2001JB000402.

Yamano, M., S. Uyeda, J. Foucher, and J. Sibuet (1989), Heat flow anomaly in the middle Okinawa Trough, *Tectonophysics*, *159*, 307–318.

Yin, A., and T. M. Harrison (2000), Geologic evolution of the Himalayan-Tibetan orogen, *Annu. Rev. Earth Planet. Sci.*, *28*, 211–280.

Zang, S., and J. Ning (1996), Study on the subduction zone in western pacific and its implication for the geodynamics, *Chin. J. Geophys.*, *39*, 188–202.

Zeng, R., Z. Deng, Q. Wu, and J. Wu (2000), Seismological evidences for the multiple incomplete crustal subduction in Himalaya and southern Tibet, *Chin. J. Geophys.*, *43*, 780–797.

Zhang, Y., and T. Tanimoto (1993), High-resolution global upper mantle structure and plate tectonics, *J. Geophys. Res.*, *98*, 9793–9823.

Zhao, D. (2001), Seismic structure and origin of hotspots and mantle plumes, *Earth Planet. Sci. Lett.*, *192*, 251–265.

Zhao, D. (2004), Global tomographic images of mantle plumes and subducting slabs: Insight into deep Earth dynamics, *Phys. Earth Planet. Inter.*, *146*, 3–34.

Zhao, D., and J. Lei (2004), Seismic ray path variations in a 3-D global velocity model, *Phys. Earth Planet. Inter.*, *141*, 153–166.

Zhao, D., A. Hasegawa, and S. Horiuchi (1992), Tomographic imaging of P and S wave velocity structure beneath northeastern Japan, *J. Geophys. Res.*, *97*, 19,909–19,928.

Zhao, D., A. Hasegawa, and H. Kanamori (1994), Deep structure of Japan subduction zone as derived from local, regional and teleseismic events, *J. Geophys. Res.*, *99*, 22,313–22,329.

Zhao, D., Y. Xu, D. Wiens, L. Dorman, J. Hildebrand, and S. Webb (1997), Depth extent of the Lau back-arc spreading center and its relation to subduction processes, *Science*, *278*, 254–257.

Zhao, D., K. Asamori, and H. Iwamori (2000), Seismic structure and magmatism of the young Kyushu subduction zone, *Geophys. Res. Lett.*, *27*, 2057–2060.

Zhao, D., O. P. Mishra, and R. Sanda (2002), Influence of fluids and magma on earthquakes: Seismological evidence, *Phys. Earth Planet. Inter.*, *132*, 249–267.

Zhao, D., J. Lei, and Y. Tang (2004), Origin of the Changbai volcano in northeast China: Evidence from seismic tomography, *Chin. Sci. Bull.*, *49*, 1401–1408.

Zhao, W., K. Nelson, and INDEPTH Project Team (1993), Deep seismic reflection evidence for continental underthrusting beneath southern Tibet, *Nature*, *366*, 557–559.

Zhao, W., K. Nelson, Z. Xu, L. Brown, J. Kol, R. Meissner, J. Xiong, and INDEPTH Project Team (1997), Double intracontinental underthrusting structure of the Yarlung Zangbo suture and different molten layers, *Chin. J. Geophys.*, *40*, 325–336.

Zhao, Z., and B. F. Windley (1990), Cenozoic tectonic extension and inversion of the Jizhong basin, Hebei, northern China, *Tectonophysics*, *185*, 83–89.

Zhou, H. (1996), A high-resolution P wave model for top 1200 km of the mantle, *J. Geophys. Res.*, *101*, 27,791–27,810.

Zhou, H., and R. Clayton (1990), P and S wave travel-time inversions for subducting slab under the island arcs of the northwest Pacific, *J. Geophys. Res.*, *95*, 6829–6851.

Zhu, L., Q. Xu, and X. Chen (2002), Group velocity of Rayleigh wave in Chinese continent and its adjacent seas, *Chin. J. Geophys.*, *45*, 491–501.

J. Huang, Institute of Earthquake Science, China Earthquake Administration, Beijing 100036, China. (hjl@seis.ac.cn)

D. Zhao, Geodynamics Research Center, Ehime University, Matsuyama 790-8577, Japan. (zhao@sci.ehime-u.ac.jp)